0.1% sodium dodecyl sulfate, 100 μg ml^{-1} phenylmethylsulfonyl fluoride, 1 mM sodium orthovanadate, and protease inhibitor cocktail) for western blotting analysis.

Cell culture

Murine primary dermal fibroblasts from the skin of four newborn WT and four newborn $PN^{-/-}$ mice were isolated and cultured as previously described (Terao *et al.*, 2010). Human primary dermal fibroblasts were purchased from DS Pharma Biomedical (Osaka, Japan). After 24 hours of serum starvation, dermal fibroblasts at confluence were treated with 0.1 to 100 μM histamine (Sigma–Aldrich, Tokyo, Japan) or 100 ng ml^{-1} recombinant mouse periostin (rmPeriostin, R&D Systems, Minneapolis, MN) for the indicated periods of time before extraction of RNA and protein. Cells were used at passage three. In each experiment, the obtained fibroblasts were examined at the same time point and under the same culture conditions (e.g., cell density, passage, and days after plating). For inhibition experiments, fibroblasts were preincubated for 2 hours with specific histamine receptor antagonists (Pyrilamine maleate, Cimetidine, JNJ7777120, 100 mM, Sigma–Aldrich) or ERK1/2 inhibitor (U0126, 20 μM, Cell Signaling Technology, Beverly, MA) before the addition of histamine. We performed serial dilutions of each agent to identify the most effective concentrations to be used in the experiments, as determined by MTT assays and western blotting analyses.

Quantitative real-time and direct reverse transcriptase–PCR analysis of mRNA

Total RNA was isolated from fibroblasts using the RNeasy Mini Kit (QIAGEN, Tokyo, Japan) according to the manufacturer's protocol. First, 100 ng of RNA was reverse-transcribed using the QuantiTect Reverse Transcription Kit (QIAGEN). For quantitative real-time reverse transcriptase–PCR analysis, standard curves for periostin, collagen, and glyceraldehyde 3-phosphate dehydrogenase (GAPDH) were generated from serial dilutions of positively expressing cDNA. Relative quantification of the PCR products was carried out using the ABI prism 7000 (Applied Biosystems, Darmstadt, Germany) and the comparative threshold cycle (C_T) method. The "fold-induction" was calculated as the ratio to values of cells that were not incubated with histamine or periostin. The primers used for real-time PCR were as follows: periostin, sense 5′-GAACGAATCATTACAGGTCC-3′, antisense 5′-GGAGACCTCTTTTTGCAAGA-3′; collagen type-I alpha 1 (Col1-α1), sense 5′-GAGCCCTCGCTTCCGTACTC-3′, antisense 5′-TGTTCCCTACTCAGCCGTCTGT-3′; and GAPDH, sense 5′-TGTC ATCATACTTGGCAGGTTTCT-3′, antisense 5′-CATGGCCTTCCGTG TTCCTA-3′. Each reaction was performed in triplicate. Variation within samples was less than 10%. Statistical analysis was performed with the Student's paired *t*-test.

Western blotting analyses

For preparation of protein samples, cell pellets and skin samples were extracted as described above, and 5 μg of extracted protein was used for western blotting analysis, as described previously (Terao *et al.*, 2010). The primary antibodies were used at the following dilutions: anti-type I collagen (Calbiochem, San Diego, CA) at 1:500, anti-periostin (R&D Systems, Minneapolis, MN) at 1:500, anti-phospho-ERK1/2 (Cell Signaling Technology) at 1:1,000, anti-total ERK1/2 (Cell Signaling Technology) at 1:1,000, anti-phospho-CREB (Cell Signaling Technology) at 1:1,000, anti-total CREB (Cell Signaling Technology) at 1:1,000, and anti-GAPDH (Santa Cruz Biotechnology, Santa Cruz, CA) at 1:500. Staining with the anti-GAPDH antibody was used as a loading control. Signal intensity of bands was quantified using the ImageJ densitometry software (http://rsb.info.nih.gov/ij/index.html) and normalized to GAPDH signal intensity.

Sircol collagen assay

The soluble collagen levels in culture supernatants were measured using a Sircol Collagen Assay (Biocolor, Belfast, UK). This assay measured total secreted collagen from cultured cells. Briefly, cells were cultured for 48 hours with or without treatment, and then supernatants were collected. One milliliter of Sirius red, an anionic dye that specifically reacts with the basic side chain groups of collagens, was added to 200 μl of the supernatant and incubated with gentle rotation for 30 minutes at room temperature. After centrifugation, the collagen-bound dye was resolubilized in 1 ml of 0.5 M NaOH, and the absorbance at 540 nm was measured.

Phosphorylated kinase array

Phosphorylated kinase was profiled with the Proteome Profiler Human Phospho-Kinase Array Kit (R&D Systems). The procedures were performed according to the manufacturer's protocol using 300 μg of protein lysate per array.

Statistical analysis

All experiments reported in this paper were repeated at least three times, yielding similar results, and data are presented as mean ± SD. The Student's two-tailed *t*-test (Microsoft Excel software, Redmond, WA) was used for comparison between two groups. When analysis included more than two groups, one-way analysis of variance (ANOVA) followed by Dunnett's test was used. *P*-values less than 0.05 were considered statistically significant.

CONFLICT OF INTEREST

The authors state no conflict of interest.

ACKNOWLEDGMENTS

We thank Kenju Nishida for excellent technical support. This study was partly supported by a research grant from the Ministry of Health, Labour and Welfare, Japan.

SUPPLEMENTARY MATERIAL

Supplementary material is linked to the online version of the paper at http://www.nature.com/jid

REFERENCES

Artuc M, Hermes B, Steckelings UM *et al.* (1999) Mast cells and their mediators in cutaneous wound healing–active participants or innocent bystanders? *Exp Dermatol* 8:1–16

Asano M, Kubota S, Nakanishi T *et al.* (2005) Effect of connective tissue growth factor (CCN2/CTGF) on proliferation and differentiation of mouse periodontal ligament-derived cells. *Cell Commun Signal* 3:11

Atkins FM, Clark RA (1987) Mast cells and fibrosis. *Arch Dermatol* 123:191–3

Baiardini I, Giardini A, Pasquali M *et al.* (2003) Quality of life and patients' satisfaction in chronic urticaria and respiratory allergy. *Allergy* 58:621–3

Banerjee I, Fuseler JW, Intwala AR *et al.* (2009) IL-6 loss causes ventricular dysfunction, fibrosis, reduced capillary density, and dramatically alters the cell populations of the developing and adult heart. *Am J Physiol Heart Circ Physiol* 296:H1694–704

Baril P, Gangeswaran R, Mahon PC *et al.* (2007) Periostin promotes invasiveness and resistance of pancreatic cancer cells to hypoxia-induced cell death: role of the beta4 integrin and the PI3k pathway. *Oncogene* 26:2082–94

Blanchard C, Mingler MK, McBride M *et al.* (2008) Periostin facilitates eosinophil tissue infiltration in allergic lung and esophageal responses. *Mucosal Immunol* 1:289–96

Cohen IK, Beaven MA, Horáková Z *et al.* (1972) Histamine and collagen synthesis in keloid and hypertrophic scar. *Surg Forum* 23:509–10

Coutu DL, Wu JH, Monette A *et al.* (2008) Periostin, a member of a novel family of vitamin K-dependent proteins, is expressed by mesenchymal stromal cells. *J Biol Chem* 283:17991–8001

Davies MG, Greaves MW (1980) Sensory responses of human skin to synthetic histamine analogues and histamine. *Br J Clin Pharmacol* 9:461–5

Dorn GW (2007) Periostin and myocardial repair, regeneration, and recovery. *N Engl J Med* 357:1552–4

Elliott CG, Wang J, Guo X *et al.* (2012) Periostin modulates myofibroblast differentiation during full-thickness cutaneous wound repair. *J Cell Sci* 125:121–32

Gailit J, Marchese MJ, Kew RR *et al.* (2001) The differentiation and function of myofibroblasts is regulated by mast cell mediators. *J Invest Dermatol* 117:1113–9

Hawkins RA, Claman HN, Clark RA *et al.* (1985) Increased dermal mast cell populations in progressive systemic sclerosis: a link in chronic fibrosis? *Ann Intern Med* 102:182–6

Hebda PA, Collins MA, Tharp MD (1993) Mast cell and myofibroblast in wound healing. *Dermatol Clin* 11:685–96

Hoffjan S, Epplen JT (2005) The genetics of atopic dermatitis: recent findings and future options. *J Mol Med (Berl)* 83:682–92

Horiuchi K, Amizuka N, Takeshita S *et al.* (1999) Identification and characterization of a novel protein, periostin, with restricted expression to periosteum and periodontal ligament and increased expression by transforming growth factor beta. *J Bone Miner Res* 14:1239–49

Hur DG, Khalmuratova R, Ahn SK *et al.* (2012) Roles of periostin in symptom manifestation and airway remodeling in a murine model of allergic rhinitis. *Allergy Asthma Immunol Res* 4:222–30

Iekushi K, Taniyama Y, Azuma J *et al.* (2007) Novel mechanisms of valsartan on the treatment of acute myocardial infarction through inhibition of the antiadhesion molecule periostin. *Hypertension* 49:1409–14

Kawashima M, Harada S, Tango T (2002) Review of fexofenadine in the treatment of chronic idiopathic urticaria. *Int J Dermatol* 41:701–6

Kudo Y, Iizuka S, Yoshida M *et al.* (2012) Periostin directly and indirectly promotes tumor lymphangiogenesis of head and neck cancer. *PLoS One* 7:e44488

Lee JH, Chen SY, Yu CH *et al.* (2009) Noninvasive *in vitro* and *in vivo* assessment of epidermal hyperkeratosis and dermal fibrosis in atopic dermatitis. *J Biomed Opt* 14:014008

Leung DY (1995) Atopic dermatitis: the skin as a window into the pathogenesis of chronic allergic diseases. *J Allergy Clin Immunol* 96:302–18

Masuoka M, Shiraishi H, Ohta S *et al.* (2012) Periostin promotes chronic allergic inflammation in response to Th2 cytokines. *J Clin Invest* 122:2590–600

Meltzer EO, Casale TB, Nathan RA *et al.* (1999) Once-daily fexofenadine HCl improves quality of life and reduces work and activity impairment in patients with seasonal allergic rhinitis. *Ann Allergy Asthma Immunol* 83:311–7

Murakami T, Yoshioka M, Yumoto R *et al.* (1998) Topical delivery of keloid therapeutic drug, tranilast, by combined use of oleic acid and propylene glycol as a penetration enhancer: evaluation by skin microdialysis in rats. *J Pharm Pharmacol* 50:49–54

Murota H, Bae S, Hamasaki Y *et al.* (2008) Emedastine difumarate inhibits histamine-induced collagen synthesis in dermal fibroblasts. *J Invest Allergol Clin Immunol* 18:245–52

Murota H, Katayama I (2009) Emedastine difumarate: a review of its potential ameliorating effect for tissue remodeling in allergic diseases. *Expert Opin Pharmacother* 10:1859–67

Nishioka K, Katayama I, Doi T (1987) Histamine release by scratching inflamed skin. *J Dermatol* 14:284–5

Nishiyama T, Kii I, Kashima TG *et al.* (2011) Delayed re-epithelialization in periostin-deficient mice during cutaneous wound healing. *PLoS One* 6:e18410

Noli C, Miolo A (2001) The mast cell in wound healing. *Vet Dermatol* 12:303–13

Norris RA, Moreno-Rodriguez R, Hoffman S *et al.* (2009) The many facets of the matricelluar protein periostin during cardiac development, remodeling, and pathophysiology. *J Cell Commun Signal* 3:275–86

Numata Y, Terui T, Okuyama R *et al.* (2006) The accelerating effect of histamine on the cutaneous wound-healing process through the action of basic fibroblast growth factor. *J Invest Dermatol* 126:1403–9

Oka T, Xu J, Kaiser RA *et al.* (2007) Genetic manipulation of periostin expression reveals a role in cardiac hypertrophy and ventricular remodeling. *Circ Res* 101:313–21

Okamoto M, Hoshino T, Kitasato Y *et al.* (2011) Periostin, a matrix protein, is a novel biomarker for idiopathic interstitial pneumonias. *Eur Respir J* 37:1119–27

Oku E, Kanaji T, Takata Y *et al.* (2008) Periostin and bone marrow fibrosis. *Int J Hematol* 88:57–63

Ontsuka K, Kotobuki Y, Shiraishi H *et al.* (2012) Periostin, a matricellular protein, accelerates cutaneous wound repair by activating dermal fibroblasts. *Exp Dermatol* 21:331–6

Russel JD, Russell SB, Trupin KM (1977) The effect of histamine on the growth of cultured fibroblasts isolated from normal and keloid tissue. *J Cell Physiol* 93:389–93

Sandberg N (1962) Accelerated collagen formation and histamine. *Nature* 194:183

Sandberg N (1964) Enhanced rate of healing in rats with an increased rate of histamine formation. *Acta Chir Scand* 127:9–21

Shimazaki M, Kudo A (2008) Impaired capsule formation of tumors in periostin-null mice. *Biochem Biophys Res Commun* 367:736–42

Shimazaki M, Nakamura K, Kii I *et al.* (2008) Periostin is essential for cardiac healing after acute myocardial infarction. *J Exp Med* 205:295–303

Siriwardena BS, Kudo Y, Ogawa I *et al.* (2006) Periostin is frequently overexpressed and enhances invasion and angiogenesis in oral cancer. *Br J Cancer* 95:1396–403

Spector SL, Shikiar R, Harding G *et al.* (2007) The effect of fexofenadine hydrochloride on productivity and quality of life in patients with chronic idiopathic urticaria. *Cutis* 79:157–62

Takayama G, Arima K, Kanaji T *et al.* (2006) Periostin: a novel component of subepithelial fibrosis of bronchial asthma downstream of IL-4 and IL-13 signals. *J Allergy Clin Immunol* 118:98–104

Terao M, Murota H, Kitaba S *et al.* (2010) Tumor necrosis factor-alpha processing inhibitor-1 inhibits skin fibrosis in a bleomycin-induced murine model of scleroderma. *Exp Dermatol* 19:38–43

Thompson AK, Finn AF, Schoenwetter WF (2000) Effect of 60 mg twice-daily fexofenadine HCl on quality of life, work and classroom productivity, and regular activity in patients with chronic idiopathic urticaria. *J Am Acad Dermatol* 43:24–30

Topol BM, Lewis VL, Benveniste K (1981) The use of antihistamine to retard the growth of fibroblasts derived from human skin, scar, and keloid. *Plast Reconstr Surg* 68:227–32

Trautmann A, Toksoy A, Engelhardt E *et al.* (2000) Mast cell involvement in normal human skin wound healing: expression of monocyte chemoattractant protein-1 is correlated with recruitment of mast cells which synthesize interleukin-4 *in vivo*. *J Pathol* 190:100–6

Wahlgren CF (1999) Itch and atopic dermatitis: an overview. *J Dermatol* 26:770–9

Weller K, Foitzik K, Paus R *et al.* (2006) Mast cells are required for normal healing of skin wounds in mice. *FASEB J* 20:2366–8

Wood SH, Clements DN, Ollier WE *et al.* (2009a) Gene expression in canine atopic dermatitis and correlation with clinical severity scores. *J Dermatol Sci* 55:27–33

Wood SH, Ke X, Nuttall T *et al.* (2009b) Genome-wide association analysis of canine atopic dermatitis and identification of disease related SNPs. *Immunogenetics* 61:765–72

Yang L, Serada S, Fujimoto M *et al.* (2012) Periostin facilitates skin sclerosis via PI3K/Akt dependent mechanism in a mouse model of scleroderma. *PLoS One* 7:e41994

IJC
International Journal of Cancer

Annexin A4-conferred platinum resistance is mediated by the copper transporter ATP7A

Shinya Matsuzaki[1,2], Takayuki Enomoto[3], Satoshi Serada[2], Kiyoshi Yoshino[1], Shushi Nagamori[4], Akiko Morimoto[1], Takuhei Yokoyama[1,2], Ayako Kim[2], Toshihiro Kimura[1], Yutaka Ueda[1], Masami Fujita[1], Minoru Fujimoto[2], Yoshikatsu Kanai[4], Tadashi Kimura[1] and Tetsuji Naka[2]

[1] Department of Obstetrics and Gynecology, Osaka University Graduate School of Medicine, Osaka, Japan
[2] Laboratory for Immune Signal, National Institute of Biomedical Innovation, Osaka, Japan
[3] Department of Obstetrics and Gynecology, Niigata University Graduate School of Medicine, Niigata, Japan
[4] Department of Pharmacology, Osaka University Graduate School of Medicine, Osaka, Japan

Although platinum drugs are often used for the chemotherapy of human cancers, platinum resistance is a major issue and may preclude their use in some cases. We recently reported that enhanced expression of Annexin A4 (Anx A4) increases chemoresistance to carboplatin through increased extracellular efflux of the drug. However, the precise mechanisms underlying that chemoresistance and the relationship of Anx A4 to platinum resistance *in vivo* remain unclear. In this report, the *in vitro* mechanism of platinum resistance induced by Anx A4 was investigated in endometrial carcinoma cells (HEC1 cells) with low expression of Anx A4. Forced expression of Anx A4 in HEC1 cells resulted in chemoresistance to platinum drugs. In addition, HEC1 control cells were compared with Anx A4-overexpressing HEC1 cells in xenografted mice. Significantly greater chemoresistance to cisplatin was observed *in vivo* in Anx A4-overexpressing xenografted mice. Immunofluorescence analysis revealed that exposure to platinum drugs induced relocation of Anx A4 from the cytoplasm to the cellular membrane, where it became colocalized with ATP7A, a copper transporter also well known as a mechanism of platinum efflux. ATP7A expression suppressed by small interfering RNA had no effect on HEC1 control cells in terms of chemosensitivity to platinum drugs. However, suppression of ATP7A in Anx A4-overexpressing platinum-resistant cells improved chemosensitivity to platinum drugs (but not to 5-fluorouracil) to a level comparable to that of control cells. These results indicate that enhanced expression of Anx A4 confers platinum resistance by promoting efflux of platinum drugs *via* ATP7A.

Platinum drugs, widely used for treating gynecological cancers, can improve survival rates dramatically, particularly in patients with ovarian and endometrial carcinomas.[1–6] Compared with platinum-sensitive tumors, prognosis is poorer for tumors that are (or become) platinum-resistant; for these tumors, other chemotherapeutic drugs also tend to be less effective. For example, an efficacy of 81% has been demonstrated for chemotherapy regimens that include platinum drugs for treatment of ovarian serous adenocarcinoma (SAC), the most common subtype of ovarian carcinoma; however, the efficacy of these regimens is only 18% for ovarian clear cell carcinomas (CCC), which are frequently resistant to multiple drugs.[7] Compared with advanced SAC, the clinical prognosis of patients with similarly advanced CCC is markedly worse largely because of the considerably higher rate of recurrence after CCC treatment.[7–11] Therefore, determining the mechanism underlying platinum resistance may aid in identification of therapeutic targets for platinum-resistant tumors such as CCC. Studies using proteomic screening approaches have previously demonstrated overexpression of Annexin A4 (Anx A4) protein in ovarian CCC, which is frequently a highly platinum-resistant tumor compared with SAC.[12] Similar findings have been reported in a study comparing SAC and CCC using a genomic screening approach.[13] Anx A4, a previously understudied member of the Annexin protein family, binds to phospholipids in a Ca^{2+}-dependent manner, self-associates on phospholipid

Key words: Annexin A4, ATP7A, platinum resistance, platinum transporter, copper transporter
Abbreviations: 5-FU: 5-fluorouracil; Anx A4: Annexin A4; CCC: clear cell carcinoma; D-MEM: Dulbecco's modified Eagle's medium; FBS: fetal bovine serum; PBS: phosphate-buffered saline; SAC: serous adenocarcinoma; siRNA: small interfering RNA
Additional Supporting Information may be found in the online version of this article.
Grant sponsor: Japanese Ministry of Education, Science, Culture and Sports; **Grant number:** 22791560; **Grant sponsors:** Program for Promotion of Fundamental Studies in Health Sciences of the National Institute of Biomedical Innovation, Ministry of Health, Labour and Welfare of Japan
DOI: 10.1002/ijc.28526
History: Received 4 Dec 2012; Accepted 26 Sep 2013; Online 8 Oct 2013
Correspondence to: Dr. Tetsuji Naka, Laboratory for Immune Signal, National Institute of Biomedical Innovation, 7-6-8 Saito-asagi, Ibaraki, Osaka 567-0085, Japan, Tel.: +81-72-641-9843, Fax: +81-72-641-9837, E-mail: tnaka@nibio.go.jp

What's new?
Although platinum-based drugs are often used in chemotherapy, resistance to these drugs is frequently a problem. The protein Annexin A4 (Anx A4) is known to be involved in platinum efflux in ovarian tumours; however, its precise mechanism of action has been unclear. In this study, the authors demonstrated that the strong platinum-resistance in Anx A4-overexpressing cells involves the transporter protein ATP7A, both in vitro and in vivo. This suggests that Anx A4 may be a highly useful therapeutic target in Anx A4-expressing carcinomas.

membrane surfaces and causes membrane aggregation.[12,14–17] Enhanced expression of Anx A4 has recently shown to increase tumor chemoresistance to carboplatin (a key drug for treating gynecological cancers) *via* increased extracellular efflux of the drug.[12] Another study showed that Anx A4 suppresses NF-κB transcriptional activity, which is significantly upregulated early after etoposide treatment. Anx A4 translocates to the nucleus together with p50 and imparts greater resistance to apoptotic stimulation by etoposide treatment.[18] Anx A4 may also be associated with drug resistance in other types of tumors; enhanced expression of Anx A4 has been reported in colon, renal, lung and pancreatic cancers.[19–23] However, the details of Anx A4-mediated extracellular efflux of platinum drugs remain unclear.

HEC1 is an endometrial carcinoma cell line with low Anx A4 expression levels. In our study, Anx A4-overexpressing derivative HEC1 cell lines were established and their chemosensitivity toward platinum drugs was analyzed both *in vitro* and *in vivo*. Anx A4-conferred platinum chemoresistance was shown to be mediated by the copper transporter ATP7A.[24–28]

Material and Methods

Cell lines

The human endometrial carcinoma cell lines HEC1, HEC1A, HEC6, HEC88nu, HEC108, HEC116 and HEC251; SNGII and SNGM cells, the human ovarian SAC cell line OVSAHO and the ovarian CCC cell lines OVISE and OVTOKO were obtained from the Japanese Collection of Research Bioresources (Osaka, Japan); A2780 cells from the human ovarian SAC cell line were obtained from the European Collection of Animal Cell Culture (Salisbury, Scotland). The identity of each cell line was confirmed by DNA fingerprinting *via* short tandem repeat profiling, as described previously.[29] HEC1, HEC1A, HEC6, HEC88nu, HEC108, HEC116 and HEC251 cells were maintained in Dulbecco's modified Eagle's medium (D-MEM) (Wako Pure Chemical Industries, Osaka, Japan) supplemented with 10% fetal bovine serum (FBS) (HyClone Laboratories, Logan, UT) and 1% penicillin–streptomycin (Nacalai Tesque, Kyoto, Japan) at 37°C under a humidified atmosphere of 5% CO_2. SNGII and SNGM cells were maintained in Ham's F12 medium (Invitrogen, Carlsbad, CA) supplemented with 10% FBS and 1% penicillin–streptomycin. OVSAHO, A2780, OVISE and OVTOKO cells were maintained in Roswell Park Memorial Institute 1640 medium (Wako Pure Chemical Industries) supplemented with 10% FBS and 1% penicillin–streptomycin.

Generation of Anx A4 stably transfected cell lines

To generate cell lines that stably expressed Anx A4, HEC1 cells were transfected with the pcDNA3.1–Anx A4 expression plasmid, as described previously.[12] Transfected cells were selected with 600 μg/ml of Geneticin (Invitrogen). Clones were maintained in 250 μg/ml of Geneticin for stability of expression. Four stable Anx A4-expressing cell lines were established and designated HEC1-A25, HEC1-A43, HEC1-A63 and HEC1-A77. A control cell line of HEC1 was also established and stably transfected with an empty vector. This cell line was designated as HEC1-CV.

Western blotting

Cells were lysed in radioimmunoprecipitation assay buffer [10 mM Tris-HCl, pH 7.5, 150 mM NaCl, 1% Nonidet P-40, 0.5% sodium deoxycholate, 0.1% sodium dodecyl sulfate, 1% protease-inhibitor cocktail (Nacalai Tesque) and 1% phosphatase-inhibitor cocktail (Nacalai Tesque)]. After centrifugation (13,200 rpm, 4°C, 15 min), soluble proteins in the supernatant were separated using sodium dodecyl sulfate-polyacrylamide gel electrophoresis, as described previously.[12] Additional information can be found in Supporting Information Material and Methods.

Measurement of IC_{50} values after treatment with cisplatin or carboplatin

Cells were suspended in D-MEM medium supplemented with 10% FBS and were seeded in 96-well plates (2,000 cells per well) (Costar; Corning, Corning, NY) for 24 hr. They were then exposed to various concentrations of carboplatin (0–500 μM), cisplatin (0–100 μM) or 5-fluorouracil (5-FU) (0–50 μM) for 72 hr. Cell proliferation was evaluated using the WST-8 assay (Cell Counting Kit-SF; Nacalai Tesque) after treatment at the time points indicated by the manufacturer. The absorption of WST-8 was measured at a wavelength of 450 nm (reference wavelength: 630 nm) using a Model 680 microplate reader (Bio-Rad Laboratories, Hercules, CA). Absorbance values for treated cells indicative of proliferation rates were expressed as percentages relative to results for untreated controls, and the drug concentrations resulting in a 50% inhibition of cell growth (IC_{50} values) were calculated.

Small interfering RNA transfection

Two commercial small interfering RNAs (siRNAs) against ATP7A and a nonspecific control siRNA were obtained from

Qiagen (Venlo, The Netherlands) and designated ATP7A siRNA4 and ATP7A siRNA6, respectively. For gene silencing, a specific sense strand 5′-GCAGCUUGUAGUAUUGAA ATT-3′ was used for ATP7A siRNA4, and an antisense strand 5′-UUUCAAUACUACAAGCUGCTA-3′ was also used. For ATP7A siRNA6, a specific sense strand 5′-GCGUA GCUCCAGAGGUUUATT-3′ was used, and an antisense strand 5′-UAAACCUCUGGAGCUACGCAG-3′ was also used. Cells were transfected with siRNA using Lipofectamine 2000 reagent (Invitrogen) according to the manufacturer's instructions. Selective silencing of ATP7A was confirmed by Western blot analysis.

In vivo model of cisplatin resistance

All animal experiments were conducted in accordance with the Institutional Ethical Guidelines for Animal Experimentation of our National Institute of Biomedical Innovation (Osaka, Japan). Four-week-old, female Institute of Cancer Research (ICR) nu/nu mice were obtained from Charles River Japan (Yokohama, Japan). For subcutaneous xenograft experiments, 2.5×10^6 HEC1, HEC1-CV, HEC1-A63 and HEC1-A77 cells were suspended in 100 μl of 1/1 (v/v) phosphate-buffered saline (PBS)/Matrigel (Becton Dickinson, Bedford, MA) and injected subcutaneously into the flanks of the ICR nu/nu mice ($n = 5$ per group). One week after xenograft establishment, tumors measured ~100 mm^3. Mice were then randomly divided into two groups and administered cisplatin (3 mg/kg) or PBS i.p. twice weekly for 4 weeks. Tumor volumes were determined twice weekly by measuring length (L), width (W) and depth (D). Tumor volume was calculated using the formula: tumor volume (mm^3) = $W \times L \times D$. At 56 days after tumor implantation, tumors were removed and weighed.

Quantification of intracellular platinum accumulation

Cisplatin accumulation in cells was analyzed according to a previously established method, with certain minor modifications. In brief, 6×10^6 cells (HEC1, HEC1-CV, HEC1-A25, HEC1-A43, HEC1-A63 and HEC1-A77 cells) were seeded into two 150-mm tissue culture dishes and incubated for 24 hr. The cells were then exposed to 1 mM cisplatin for 60 min at 37°C and then washed twice with PBS. After 3 hr of incubation in cisplatin-free D-MEM medium (supplemented with 10% FBS), whole extracts were prepared and the concentration of intracellular platinum was determined using an Agilent 7500ce inductively coupled plasma mass spectrometer (ICP-MS; Agilent, Santa Clara, CA). The absolute concentration of platinum in each sample was determined from a calibration curve prepared with a platinum standard solution.

Preparation of crude membrane fractions

To investigate the localization of Anx A4, crude membrane fractions (CMFs) of cells treated in various ways were prepared. Cells were divided into three groups: those that received no treatment, those pretreated with 10 μM cisplatin for 4 hr and those pretreated with 50 μM carboplatin for 4 hr. CMF were prepared as described elsewhere,[30] with modifications. Prepared proteins were investigated using Western blot analysis. Additional information can be found in Supporting Information Material and Methods.

Biotinylation of HEC1 cell membrane surface proteins after cisplatin or carboplatin exposure

To investigate the localization of ATP7A after exposure to platinum drugs, treated or mock-treated HEC1 cells were surface-biotinylated and the presence of ATP7A was investigated by Western blot analysis. Additional information can be found in Supporting Information Material and Methods.

Immunofluorescence for ATP7A and Anx A4

Immunofluorescence staining was performed 2 days after cells had been seeded on cover slips. Before staining, cells in the treatment groups were pretreated with 10 μM cisplatin or 50 μM carboplatin for 4 hr. Cells were then analyzed for localization of Anx A4 and ATP7A. Additional information can be found in Supporting Information Material and Methods.

Statistical analysis

Statistical analyses were performed using one-way analysis of variance (ANOVA) followed by Dunnett's analysis to evaluate the significance of differences. In all analyses, $p < 0.05$ was considered to be statistically significant.

Results

Expression of Anx A4 in endometrial carcinoma cell lines

To investigate Anx A4 expression in nine common endometrial carcinoma cell lines, Western blot analyses were performed. Expression of Anx A4 was strongest in SNGM cells compared with the other eight cell lines (Fig. 1*a*). Thus, enhanced expression of Anx A4 was confirmed in this endometrial carcinoma cell line.

Anx A4 and platinum resistance in HEC1 cell lines

From control HEC1 cells (low Anx A4 expression levels), four stable lines of Anx A4-overexpressing cells (HEC1-A25, HEC1-A43, HEC1-A63 and HEC1-A77 cells) and one line of empty vector transfected cells (HEC1-CV cells) were established. Overexpression of Anx A4 was confirmed using Western blot analysis and was compared with CCC cell lines (OVTOKO and OVISE) used as positive controls (Fig. 1*b*). Significantly higher IC_{50} values for cisplatin were observed in HEC1-A25 (32.1 μM, $p < 0.01$), HEC1-A43 (23.8 μM, $p < 0.01$), HEC1-A63 (34.9 μM, $p < 0.01$) and HEC1-A77 cells (17.3 μM, $p < 0.01$) compared with HEC1 (9.8 μM) and HEC1-CV cells (8.4 μM) (Fig. 1*c*). Similarly, IC_{50} values for carboplatin were significantly increased in HEC1-A25 (194.6 μM, $p < 0.01$), HEC1-A43 (153.3 μM, $p < 0.01$), HEC1-A63 (371.5 μM, $p < 0.01$) and HEC1-A77 cells (158.1 μM, $p < 0.01$) compared with HEC1 (59.1 μM) and HEC1-CV cells (60.9 μM) (Fig. 1*c*). Thus, Anx A4 overexpression conferred platinum resistance in HEC1 cell lines.

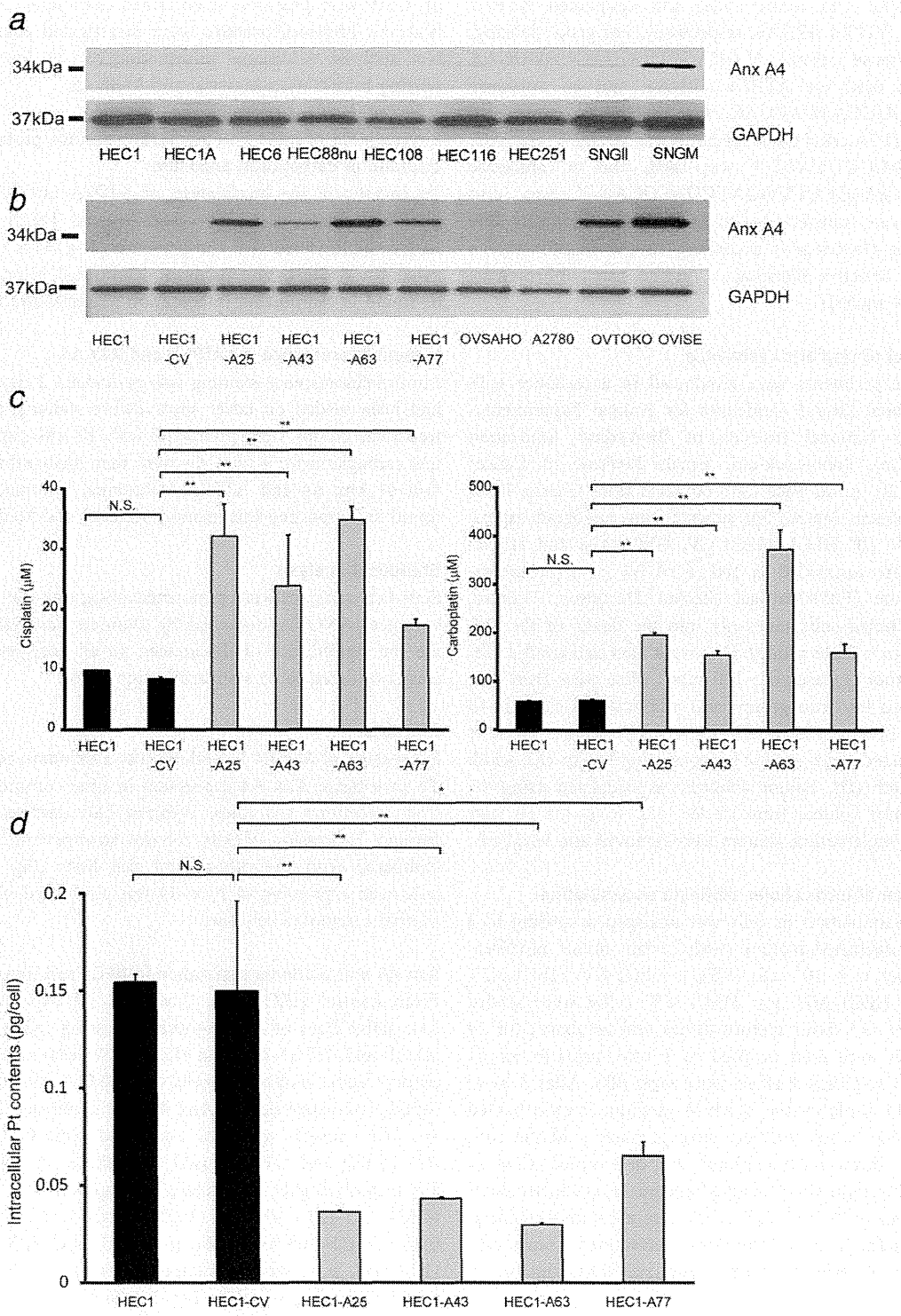

Figure 1. Enforced expression of Anx A4 in HEC1 cells confers platinum resistance *in vitro*. (*a*) Western blot analysis of nine endometrial carcinoma cell lines. Anx A4 was expressed in one cell line. (*b*) Establishment of an Anx A4-stably-expressing HEC1 cell line by transfection with the pcDNA3.1-Anx A4 expression plasmid into a HEC1 cell line with low Anx A4 expression levels. Enforced expression of Anx A4 was confirmed by Western blot analysis. (*c*) The IC_{50} sensitivity to cisplatin or carboplatin was investigated in HEC1, HEC1-CV, HEC1-A25, HEC1-A43, HEC1-A63 and HEC1-A77 cells. (*d*) Intracellular platinum accumulation was investigated after treatment with 1 mM cisplatin for 60 min and further incubation with cisplatin-free medium for 180 min and was determined by ICP-MS analysis.

Intracellular platinum accumulation in Anx A4-overexpressing cells

To elucidate the mechanism underlying platinum resistance induced by Anx A4, intracellular platinum accumulation of HEC1, HEC1-CV, HEC1-A25, HEC1-A43, HEC1-A63 and HEC1-A77 cells after cisplatin exposure was analyzed. Significantly less platinum had accumulated in HEC1-A25, HEC1-A43, HEC1-A63 and HEC1-A77 cells compared with HEC1 and HEC1-CV cells (0.036 pg/cell, $p < 0.01$; 0.04 pg/cell, $p < 0.01$; 0.03 pg/cell, $p < 0.01$; 0.065 pg/cell, $p < 0.05$ and 0.154 and 0.150 pg/cell, respectively) (Fig. 1*d*). Thus, intracellular platinum accumulation was decreased in Anx A4-overexpressing cells.

Anx A4-overexpressing cells and cisplatin in xenograft models

To determine the involvement of Anx A4 in platinum resistance *in vivo*, HEC1, HEC1-CV, HEC1-A63 and HEC1-A77 cells were subcutaneously injected into nude mice. After the tumor xenograft had been established, cisplatin or PBS was given twice a week for 1 month. On Day 56, average tumor volumes were 11,496 ± 950 mm^3 in PBS-treated HEC1-CV control mice and 3,554 ± 872 mm^3 in cisplatin-treated HEC1-CV controls. A significant antitumor effect of cisplatin was therefore observed in HEC1-CV-xenografted mice compared with the PBS-treated group. The parent HEC1 and HEC1-CV xenografts responded similarly to cisplatin (Fig. 2*a*; $p < 0.01$).

In HEC1-A63-xenografted mice, the average tumor volume on Day 56 was 8,245 ± 160 mm^3 in the PBS-treated group and only slightly less (7,078 ± 257 mm^3) in the cisplatin-treated group (Fig. 2*a*; $p = 0.42$). A similar response to cisplatin was observed in the HEC1-A63 and HEC1-A77 xenografts. On Day 56, no significant differences in tumor weight were found in HEC1-A63-xenografted mice between the PBS treatment (4.66 ± 0.42 g) and the cisplatin treatment groups (4.43 ± 0.16 g) (Fig. 2*b*). Similar results were observed in HEC1-A77 xenograft models. In contrast, a significant decrease in tumor weight was observed in HEC1-CV-xenografted mice between the PBS mock treatment (5.95 ± 1.16 g) and the cisplatin treatment groups (3.20 ± 0.76 g; $p < 0.05$) (Fig. 2*b*). Similar results were observed for the HEC1 and HEC1-CV xenografts. No significant differences in tumor weight in the PBS treatment group were observed among HEC1-CV-xenografted (5.95 ± 1.16 g), HEC1-xenografted (7.48 ± 0.34 g), HEC1-A63-xenografted (4.66 ± 0.42 g) and HEC1-A77-xenografted mice (4.82 ± 1.08 g) (Fig. 2*b*). These results indicated that overexpression of Anx A4 in HEC1 endometrial carcinoma cell lines conferred significant platinum resistance to the cells as tumors growing *in vivo*.

Translocation of Anx A4 and ATP7A after platinum exposure

In our study, platinum transporters were the focus of an investigation of the molecular mechanisms of chemoresistance induced by Anx A4. In previous research, intracellular platinum levels were decreased after enhanced expression of Anx A4, and ATP7A and ATP7B are well known as efflux transporters of platinum drugs.[27,28,31] However, the relationship of Anx A4 with ATP7A and ATP7B has not been previously examined. The results of our study demonstrated no change in expression of ATP7A at the protein levels owing to enforced overexpression of Anx A4 (Fig. 3*a*) and no ATP7B expression in HEC1 cells (data not shown). Therefore, the effects of Anx A4 expression on ATP7B in these cells were not investigated.

Because Anx A4 is normally localized to the cytoplasm, we theorized that exposure to platinum drugs may induce translocation of Anx A4 to the cellular membrane, resulting in an increase in chemoresistance owing to the influence of ATP7A. To investigate the possibility of induced translocation of Anx A4 and ATP7A by platinum drugs, CMFs were prepared. By Western blot analysis, Anx A4 expression in CMF of HEC1 and HEC1-CV cells before and after treatment with cisplatin or carboplatin was barely detectable because of its low endogenous expression in these cells (Fig. 3*b*). In contrast, Anx A4 expression was increased in CMF of HEC1-A63 cells and HEC1-A77 cells treated with cisplatin and carboplatin compared with untreated cells (Fig. 3*b*). Biotinylation-based cell surface membrane protein enrichment revealed a marked increase in biotinylation of ATP7A after exposure to cisplatin or carboplatin in HEC1, HEC1-CV, HEC1-A63 and HEC1-A77 cells (Fig. 3*c*). In the biotinylated samples, no Anx A4 expression was detected on the cell surface, although it had been previously detected in the cell CMF (data not shown). These results suggested that exposure to cisplatin or carboplatin induced massive translocation of Anx A4 to CMF, including the inner surface of the cell membrane (inaccessible to biotinylation). Before exposure of the cell to cisplatin or carboplatin, ATP7A was not expressed in biotinylated samples but after exposure, strong ATP7A expression was detected. These results suggested that exposure to cisplatin or carboplatin induced massive translocation of ATP7A to the outer surface of the cell (accessible to biotinylation).

Anx A4 and ATP7A localization

By immunofluorescence analysis, Anx A4 was localized in the perinuclear and cytoplasmic regions of untreated cells, whereas ATP7A was localized mainly in the perinuclear and cytoplasmic regions and slightly less in the cellular membrane in HEC1, HEC1-CV, HEC1-A63 and HEC1-A77 cells (Figs. 4*a*–4*d*). After 4-hr exposure to cisplatin or carboplatin, Anx A4 and ATP7A were found to be colocalized to the cellular membrane in HEC1-A63 cells (Fig. 4*c*). Similar findings were observed in HEC1-A77 cells (Fig. 4*d*). Because of the low expression of Anx A4 in HEC1 and HEC1-CV cells, no Anx A4 was detected in the cellular membranes in these cells (Figs. 4*a* and 4*b*). Thus, the results of the immunofluorescence analysis were in accordance with those of both Western blot analysis of CMF preparations and biotinylation

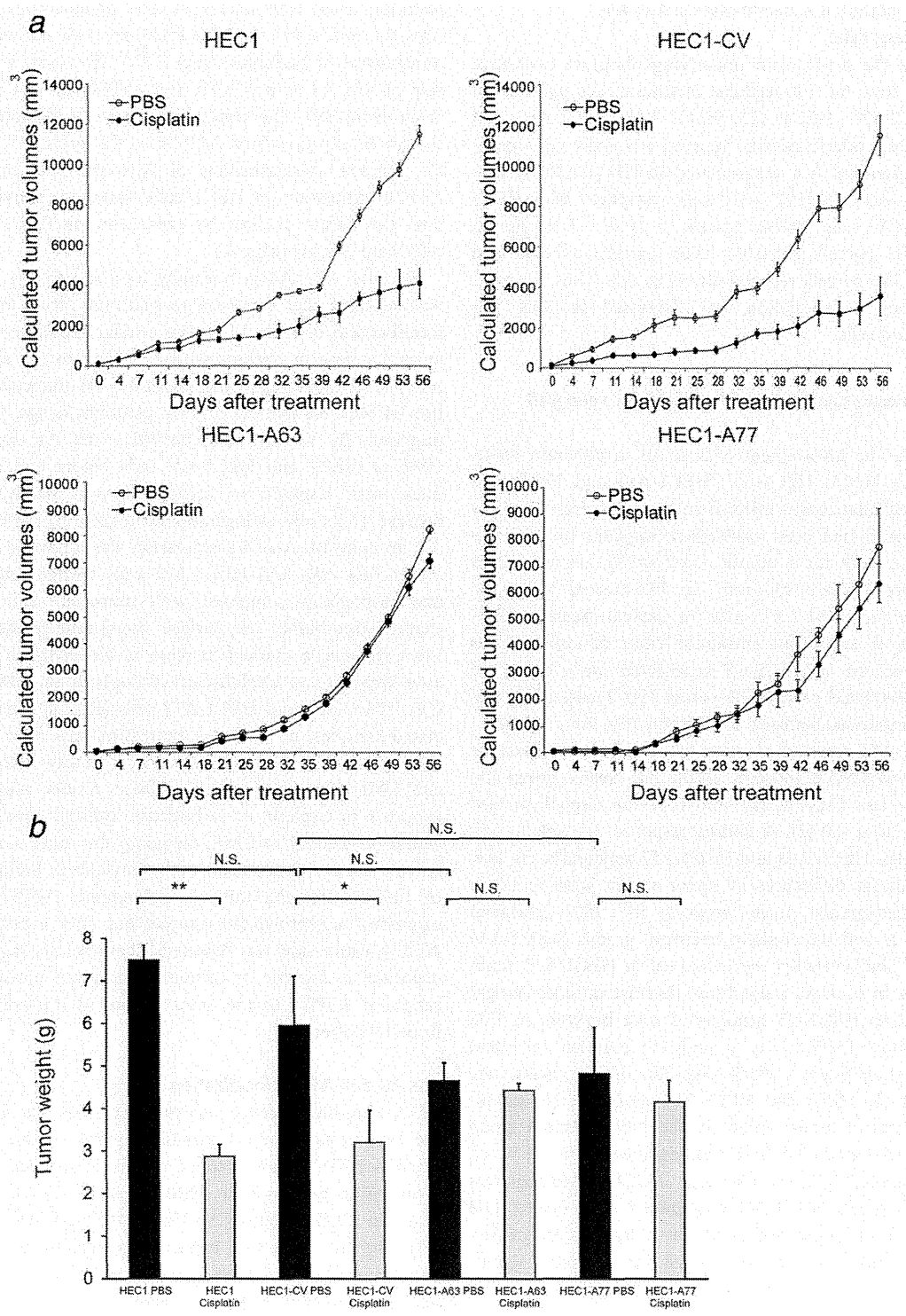

Figure 2. Enforced expression of Anx A4 in HEC1 cells confers platinum resistance *in vivo*. Analysis of Anx A4 as a platinum-resistant protein *in vivo*. (*a*) To determine the resistance of Anx A4-stably-expressing HEC1 cells to platinum *in vivo*, parent HEC1, HEC1-CV, HEC1-A63 and HEC1-A77 cells were subcutaneously injected into nude mice ($n = 5$ per group). After tumor xenografts were established, cisplatin (3 mg/kg) or PBS was administered i.p. twice weekly for 1 month. Figure shows the average (points) for five animals ± SD (bars). (*b*) Fifty-six days after implantation, tumors were removed and weighed. Values shown are the means (±SD) of five mice. NS: not significant (*$p <$ 0.05; **$p < 0.01$; one-way ANOVA, followed by Dunnett's analysis).

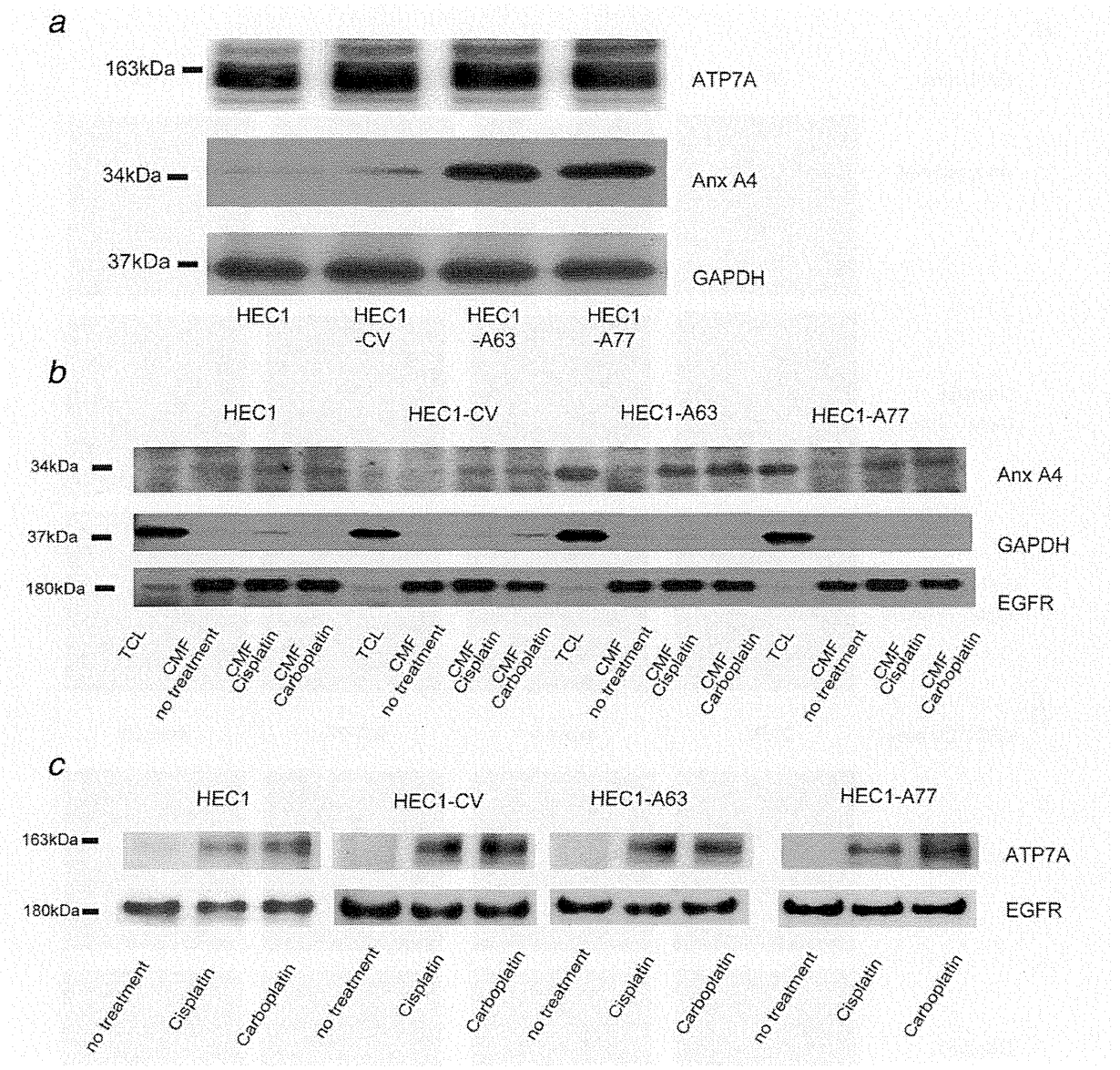

Figure 3. Localization of Anx A4 and ATP7A was investigated using Western blot analysis. The localization of Anx A4 and ATP7A was investigated using two techniques: orthogonal crude membrane fractions and biotinylation of cell surface proteins. (*a*) No significant change in expression levels of ATP7A was observed in HEC1, HEC1-CV, HEC1-A63 or HEC1-A77 cells. (*b*) In both HEC1-A63 and HEC1-A77 cells (but not in HEC1 and HEC1-CV cells), the drug-induced translocation of Anx A4 into the crude membrane fraction was shown by Western blot analysis after exposure to 10 μM cisplatin or 50 μM carboplatin for 4 hr. TCL: total cell lysate. Epidermal growth factor receptor was used as the control for cell surface protein labeling. (*c*) In HEC1, HEC1-CV, HEC1-A63 and HEC1-A77 cells, translocation of ATP7A to the cell surface was shown by Western blot analysis. Cells were treated with 25 μM cisplatin or 150 μM carboplatin for 4 hr, and cell surface proteins were biotinylated with 500 μM sulfo-NHS-SS-biotin. Biotinylated surface proteins were enriched with UltraLink Immobilized Neutroavidin (Thermo Fisher Scientific, Waltham, MA) and analyzed by Western blot analysis using anti-ATP7A. Levels of epidermal growth factor receptor, a surface protein, are shown as loading controls.

assays (Figs. 3*b* and 3*c*). Anx A4 and ATP7A were localized in the cytoplasm before cisplatin or carboplatin exposure; Anx A4 and ATP7A were then translocated to the cellular membrane after cisplatin or carboplatin exposure. Thus, Anx A4 and ATP7A are colocalized to the cellular membrane in platinum-treated HEC1-A63 and HEC1-A77 cells but not in HEC1 and HEC1-CV cells.

Effect of ATP7A expression on resistance to platinum drugs

The mechanism of platinum resistance conferred by Anx A4 overexpression was explored further by suppression of ATP7A expression using siRNA. The suppression of ATP7A was confirmed using Western blot analysis (Fig. 5*a*). Anx A4 expression was unchanged by silencing ATP7A (Fig. 5*a*). The

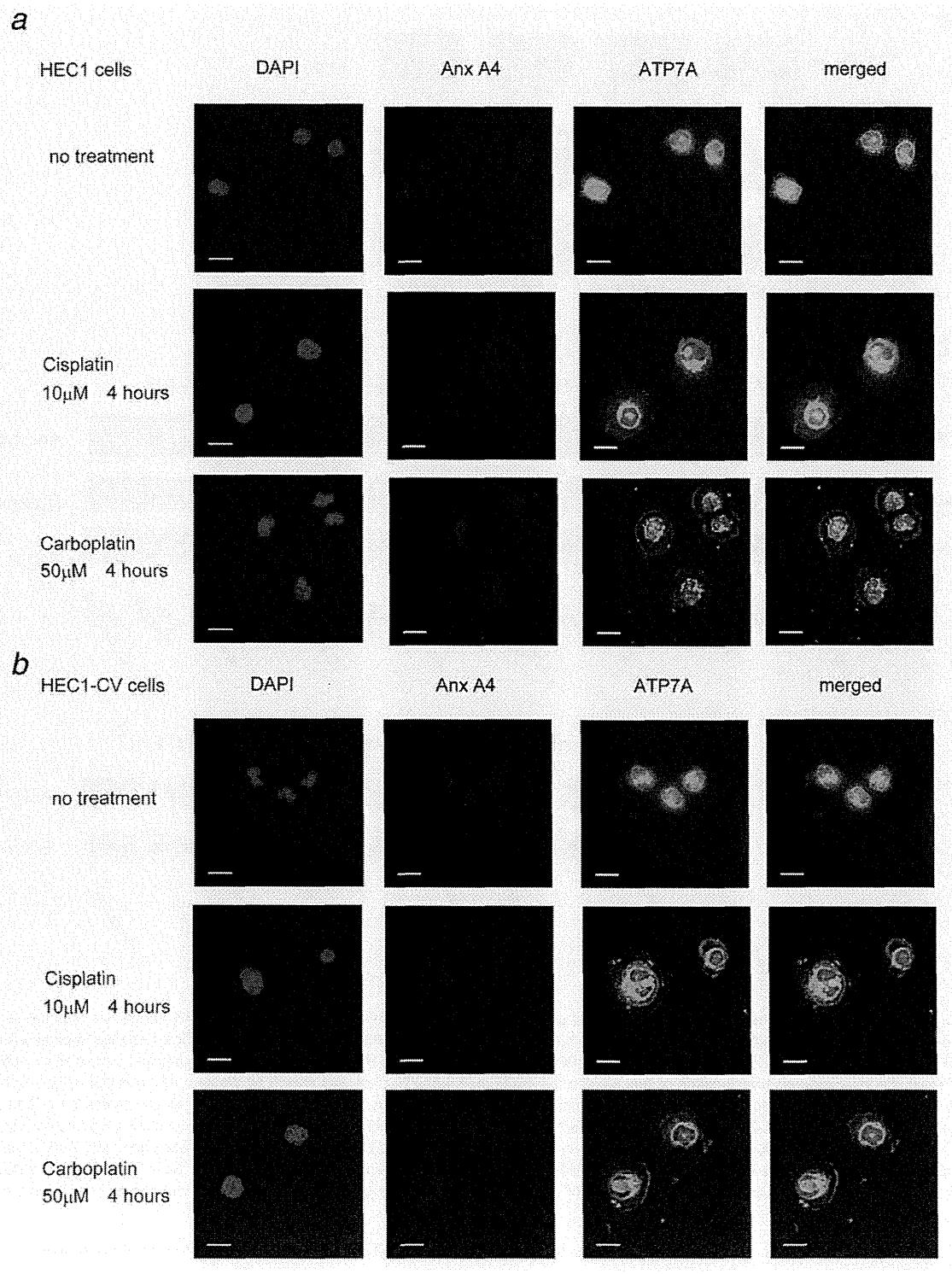

Figure 4. Immunofluorescence staining for ATP7A and Anx A4. HEC1, HEC1-CV, HEC1-A63 and HEC1-A77 cells were divided into three groups: the no treatment, cisplatin exposure and carboplatin exposure groups. (*a*) HEC1 cells, (*b*) HEC1-CV cells, (*c*) HEC1-A63 cells and (*d*) HEC1-A77 cells. Cells were incubated with anti-Anx A4 antibody (red) or anti-ATP7A antibody (green). Nuclei were stained with DAPI (blue). In the no treatment group for each cell, Anx A4 was localized in perinuclear and cytoplasmic regions and ATP7A was strongly localized in perinuclear regions. In HEC1 and HEC1-CV cells, after exposure to cisplatin or carboplatin, ATP7A was relocalized in the cellular membrane, although some ATP7A remained in the cytoplasm; however, no change in location of Anx A4 was observed. In HEC1-A63 and HEC1-A77 cells, Anx A4 and ATP7A were newly colocalized in the cellular membrane as well as remaining in the cytoplasm. In a comparison of HEC1 and HEC1-CV cells with HEC1-A63 and HEC1-A77 cells, expression of Anx A4 in HEC1-A63 and HEC1-A77 cells was stronger in the cytoplasm and cellular membrane. Scale bar = 30 μm.

Int. J. Cancer: **134**, 1796–1809 (2014) © 2013 UICC

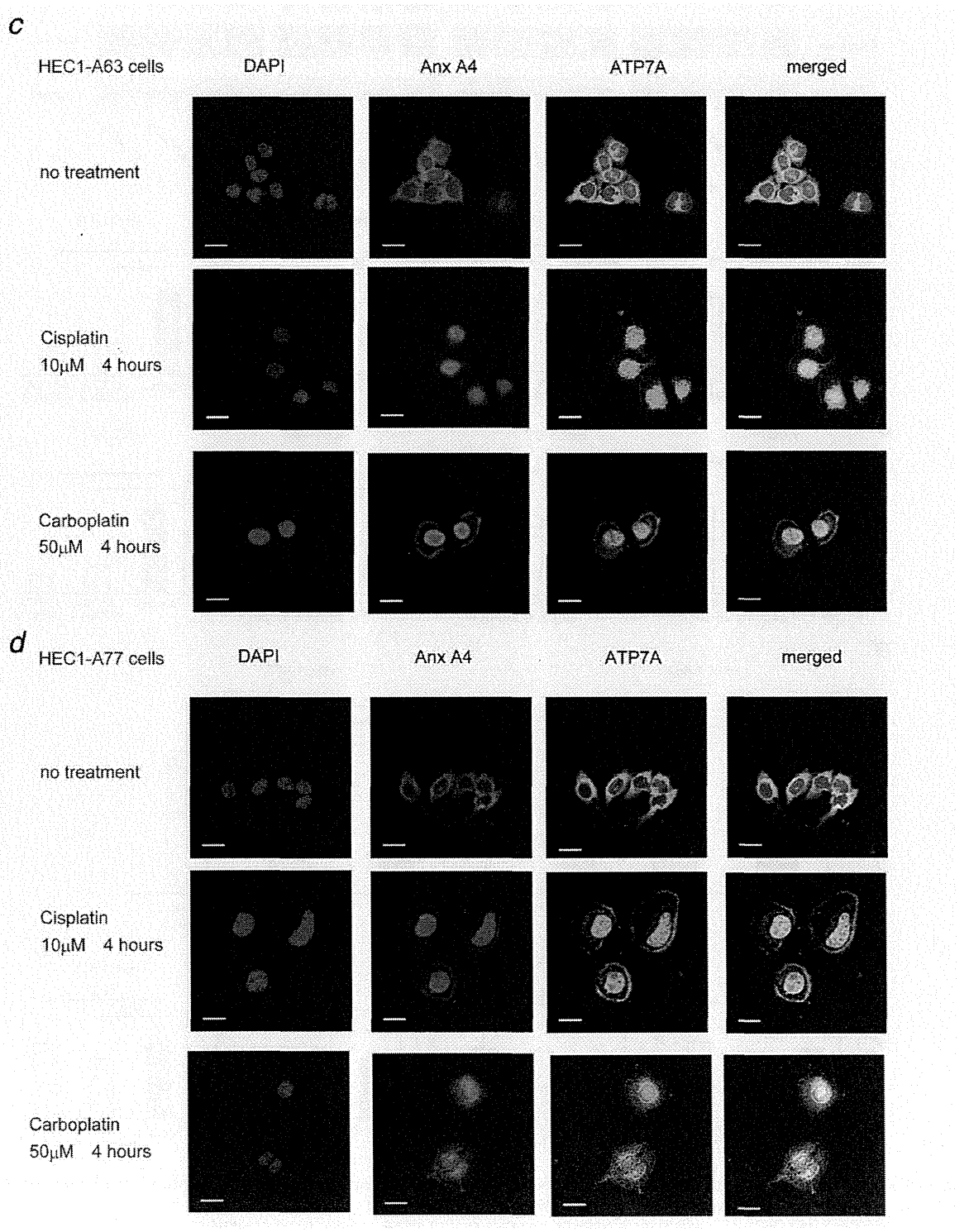

Figure 4. (Continued)

control and commercial siRNAs against ATP7A were transfected and the IC_{50} values of cisplatin and carboplatin were determined for each cell line. The IC_{50} value for cisplatin was significantly lower for the two kinds of ATP7A-silenced HEC1-A63 cells (ATP7A siRNA4, $IC_{50} = 11.0$ μM, $p < 0.01$; ATP7A siRNA6, $IC_{50} = 11.2$ μM, $p < 0.01$) compared with

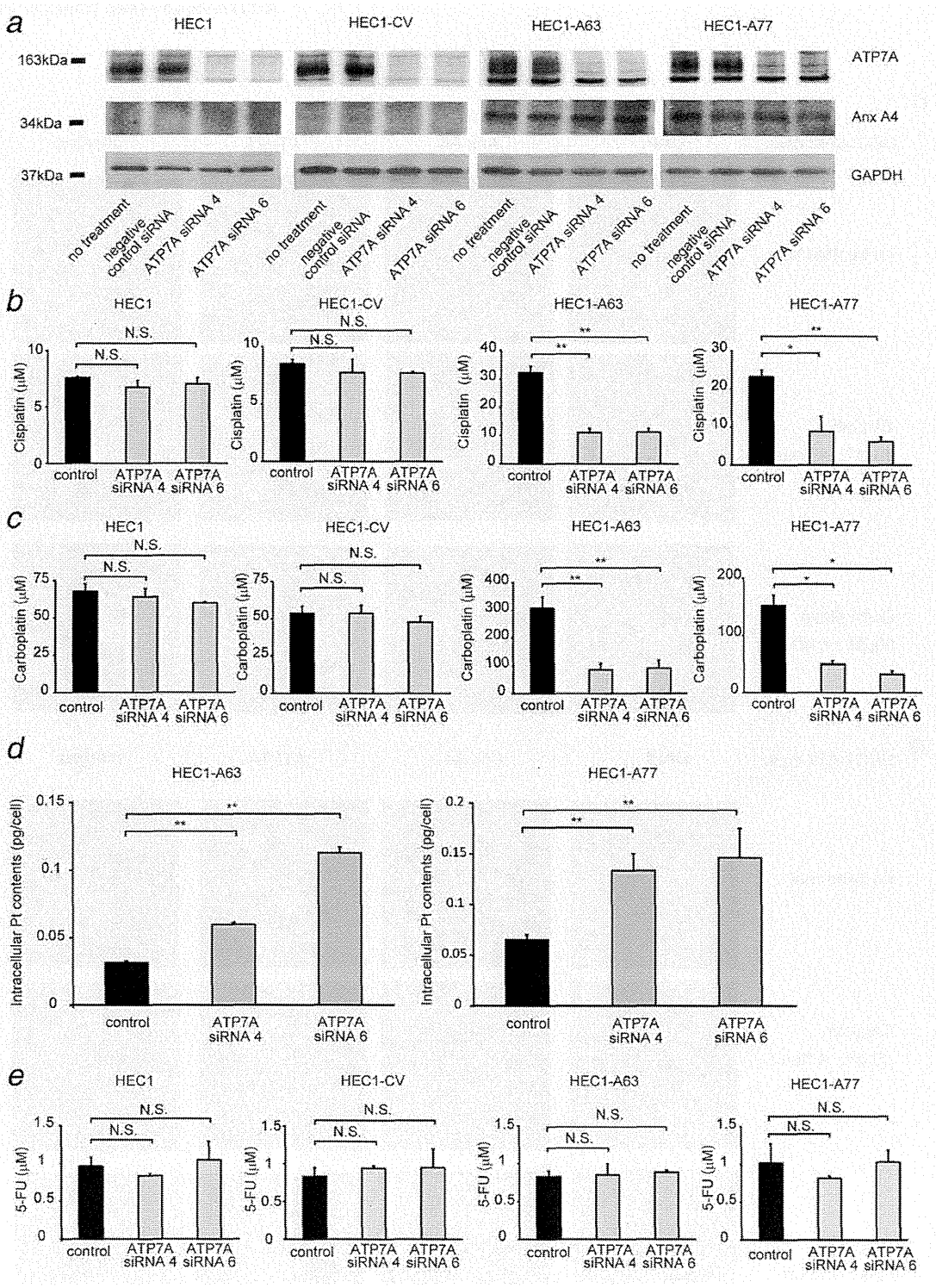

Figure 5. Knockdown of ATP7A expression improves platinum chemosensitivity in Anx A4-overexpressing cells. (*a*) Knockdown expression of ATP7A by siRNA in HEC1, HEC1-CV, HEC1-A63 and HEC1-A77 cells by Western blot analysis. (*b*) IC_{50} values are shown for cisplatin in HEC1, HEC1-CV, HEC1-A63 and HEC1-A77 cells transfected with negative control siRNA and two types of siRNA targeting ATP7A. A significant decrease in IC_{50} value for cisplatin was observed for the two types of ATP7A-silenced HEC1-A63 and HEC1-A77 cells but not for the HEC1 and HEC1-CV cells. (*c*) IC_{50} values are shown for carboplatin in HEC1, HEC1-CV, HEC1-A63 and HEC1-A77 cells transfected with negative control siRNA and two kinds of siRNA targeting ATP7A. A significant decrease in IC_{50} value for carboplatin was observed for the two types of ATP7A-silenced HEC1-A63 and HEC1-A77 cells but not for the HEC1 and HEC1-CV cells. (*d*) Intracellular platinum content after treatment with 1 mM cisplatin for 60 min and further incubation with cisplatin-free medium for 180 min in D-MEM medium in HEC1-A63 cells and HEC1-A77 cells transfected with negative control siRNA and ATP7A-targeting siRNA, as determined by ICP-MS analysis. Significantly higher intracellular platinum accumulation was observed in HEC1-A63 cells and HEC1-A77 ATP7A-silencing cells than in control siRNA-transfected HEC1-A63 cells and HEC1-A77 cells. (*e*) No significant differences in IC_{50} values for 5-FU were noted between HEC1, HEC1-CV, HEC1-A63 and HEC1-A77 cells. Similar results were observed in ATP7A-silenced cell lines for HEC1, HEC1-CV, HEC1-A63 and HEC1-A77 cells (*$p < 0.05$; **$p < 0.01$; one-way ANOVA followed by Dunnett's analysis).

the HEC1-A63 control siRNA-transfected cells (IC_{50} = 32.2 μM) (Fig. 5*b*).

In addition to cisplatin, improved chemosensitivity associated with ATP7A silencing was observed with carboplatin. Significantly lower IC_{50} values for carboplatin were observed in both types of ATP7A-silenced HEC1-A63 cells (siRNA4, IC_{50} = 85.9 μM, $p < 0.01$; siRNA6, IC_{50} = 92.8 μM, $p < 0.01$) compared with the HEC1-A63 control siRNA-transfected cells (IC_{50} = 300.7 μM) (Fig. 5*c*). Similar results were found for HEC1-A77 ATP7A-silenced cells, where a significantly lower IC_{50} value for cisplatin was observed (siRNA4, IC_{50} = 8.9 μM, $p < 0.05$; siRNA6, IC_{50} = 6.2 μM, $p < 0.01$) compared with that for HEC1-A77 control siRNA-transfected cells (IC_{50} = 23.3 μM). IC_{50} values for carboplatin were also significantly lower for the two kinds of ATP7A-silenced HEC1-A77 cells (siRNA4, IC_{50} = 49.8 μM, $p < 0.05$; siRNA6, IC_{50} = 31.9 μM, $p < 0.05$) compared with the HEC1-A77 control siRNA-transfected cells (IC_{50} = 152.1 μM, $p < 0.01$) (Fig. 5*c*). In contrast, siRNA treatments targeting ATP7A were ineffective in HEC1 and HEC1-CV cells treated with cisplatin or carboplatin (Figs. 5*b* and 5*c*). Intracellular platinum accumulation after cisplatin exposure was significantly increased in HEC1-A63 cells treated with ATP7A siRNA (0.060 pg/cell, $p < 0.01$ to 0.113 pg/cell, $p < 0.01$) compared with control siRNA-transfected cells (0.030 pg/cell) (Fig. 5*d*). Similarly, a significant increase in intracellular platinum accumulation was observed in HEC1-A77 cells treated with ATP7A siRNA (0.133 pg/cell, $p < 0.01$ to 0.146 pg/cell, $p < 0.01$) compared with control siRNA-transfected cells (0.065 pg/cell) (Fig. 5*d*).

To investigate the relationship between resistance to drugs other than platinum drugs and Anx A4 or ATP7A expression, IC_{50} values for 5-FU were determined for each cell line. No significant change in IC_{50} values for 5-FU was observed in HEC1 (IC_{50} = 0.96 μM), HEC1-CV (IC_{50} = 1.00 μM), HEC1-A63 (IC_{50} = 0.83 μM) or HEC1-A77 cells (IC50 = 1.01 μM) (Fig. 5*e*). Similar results were observed in the ATP7A-silenced cell lines for HEC1, HEC1-CV, HEC1-A63 and HEC1-A77 cells as well as in ATP7A-silenced cell lines (Fig. 5*e*). These results suggested that platinum resistance induced by enforced expression of Anx A4 was mainly dependent on the platinum transporter ATP7A and that expression of Anx A4 and ATP7A was unrelated to resistance to 5-FU.

Discussion

In our study, overexpression of Anx A4 in HEC1 cells decreased cell sensitivity to platinum drugs *in vitro*. Increased drug efflux was the mechanism underlying this change. In addition, an association between Anx A4 and platinum resistance was demonstrated for the first time *in vivo*. The mechanism of Anx A4-induced drug efflux may prove to be a promising therapeutic target because blockage of that mechanism may improve the prognosis of patients with Anx A4-associated platinum-resistant tumors.

Anx A4 itself is not a drug transporter, but it does bind to phospholipids in a Ca^{2+}-dependent manner and self-associates onto phospholipid membrane surfaces, causing membrane aggregation.[12,14–17] Thus, we assumed an indirect mediating effect of Anx A4 on drug efflux through an association between an unidentified drug transporter and Anx A4. Recently, MRP2 (an ABC ATPase-like multidrug-resistant protein) and ATP7A and ATP7B (two P-type Cu-transporting ATPases) were identified as platinum efflux transporters strongly associated with platinum resistance.[32,33] In an analysis of clinical gynecological samples, expression of MRP2 failed to predict tumor response to chemotherapy and did not correlate with overall survival.[34–36] In contrast, poor survival rates were associated with overexpression of ATP7A in patients with ovarian cancer.[27] Similarly, a correlation was found between ATP7B overexpression in endometrial carcinomas and an unfavorable clinical outcome in patients treated with cisplatin-based chemotherapy.[37] Therefore, we focused on the platinum transporters ATP7A and ATP7B and investigated their relationships with expression of Anx A4. In normal, unchallenged cells, ATP7A and ATP7B are localized in the Golgi apparatus and are involved in copper homeostasis, using ATP hydrolysis to transport copper ions across cellular membranes. They function in both the export of excess copper and its delivery to copper-dependent enzymes. ATP7A and ATP7B are also known to be efflux transporters of platinum drugs.[8,27,28,31,38,39] In one study, only a slight increase in expression of transfected ATP7A was seen in a human ovarian cancer cell line; however, that small increase was sufficient to confer significant resistance to cisplatin or carboplatin.[40] In a similar study in another human cisplatin-resistant ovarian cancer cell line, silencing of ATP7B by siRNA transfection resulted in a 2.5-fold decrease in cisplatin IC_{50} levels and a significant increase in DNA-platinum adduct formation.[41] Preparing CMF of treated cells facilitated the localization of Anx A4 expression in cells before and after exposure to platinum drugs. The abundance of AnxA4 in the membrane fraction along with the translocation to the membrane was increased. Using the orthogonal method of cell surface protein labeling to monitor proteins appearing on the cell surface, biotinylated ATP7A was increased after cisplatin or carboplatin exposure both in HEC1 and HEC1-CV cells (cells expressing low levels of Anx A4) and HEC1-A63 and HEC1-A77 cells (cells overexpressing Anx A4). Taken together, these results suggest that platinum drug exposure causes relocalization of Anx A4 expression to the membrane fraction and relocalization of ATP7A transporters (to a minimum) to the external surface of the cellular membrane. Unfortunately, no similar analysis of ATP7B was possible because it is not expressed in HEC1 cells (data not shown). However, in cells that express both ATP7A and ATP7B proteins, other immunofluorescence studies have shown similar changes in localization of both proteins after cisplatin exposure.[42] After cisplatin or carboplatin exposure in HEC1-A63 and HEC1-A77 Anx

A4-overexpressing cells, immunofluorescence showed that Anx A4 expression was relocated from the perinuclear and cytoplasmic Golgi regions to the cellular membrane. This relocalization was not observed in HEC1 and HEC1-CV cells, in which overexpression of Anx A4 does not occur.

ATP7A also relocates from the perinuclear and cytoplasmic regions to the cellular membrane after cisplatin or carboplatin exposure. However, this occurs both in HEC1 and HEC1-CV cells (cells expressing low levels of Anx A4) and HEC1-A63 and HEC1-A77 cells (cells overexpressing Anx A4). Although no direct interaction between ATP7A and Anx A4 was detected by coimmunoprecipitation analysis (data not shown), immunofluorescence analysis showed colocalization of ATP7A and Anx A4 at least within the cellular membrane in Anx A4-overexpressing cells. These results suggested that Anx A4 is not required for ATP7A translocation and that ATP7A translocation is unrelated to expression of Anx A4.

Translocation of Anx A4 to plasma membranes is reportedly mediated by an increase in intracellular free Ca^{2+}, which is increased by exposure to platinum drugs.[43,44] In addition to the translocation of ATP7A and Anx A4 to the plasma membrane, our results also showed translocation of ATP7A to the nucleus in HEC1 and HEC1-CV cells. Translocation to the nucleus and colocalization of both ATP7A and Anx A4 were also observed in HEC1-A63 and HEC1-A77 cells after exposure to cisplatin or carboplatin in the immunofluorescence staining analysis in our study (Fig. 4). Anx A4 translocates to the nucleus after etoposide treatment and suppresses NF-κB transcriptional activity, which induces expression of Bax, a proapoptotic Bcl-2 family protein.[18] In addition, a correlation has been reported between nuclear staining of Anx A4 and poor survival in patients with ovarian cancer.[45] However, the role of ATP7A in the nucleus and its relationship with NF-κB transcriptional activity has not been investigated. Further investigation is needed to elucidate the role of nuclear colocalization of Anx A4 and ATP7A in platinum resistance.

In our study, translational silencing of ATP7A in HEC1 and HEC1-CV (Anx A4-nonexpressing cells) and HEC1-A63 and HEC1-A77 cells (Anx A4-overexpressing cells) was performed. Western blot analysis demonstrated no detectable changes in protein expression of Anx A4 when ATP7A was silenced in any of these four cell lines.

In HEC1 and control HEC1-CV cells (low Anx A4 expression levels), IC_{50} values for cisplatin or carboplatin cells after the knockdown of ATP7A expression caused no improvement in the sensitivity of these cells to cisplatin or carboplatin. Similar results were observed in a previous study in which no improvement in sensitivity to cisplatin resulted from silencing of ATP7A in platinum-resistant or -sensitive ovarian cancer cell lines.[41] However, Mangala *et al.* reported improved sensitivity to cisplatin in both platinum-resistant ovarian cancer cells and parental cells expressing ATP7B as a result of silencing of ATP7B expression.[41] An important discovery related to ATP7A was communicated in our study: in cells overexpressing both Anx A4 and ATP7A, silencing of ATP7A significantly improved sensitivity to cisplatin and carboplatin, thus restoring them to sensitivity levels comparable to those of HEC1 and HEC1-CV cells. These results were supported by a quantitative analysis of the accumulation of intracellular platinum, demonstrating that siRNA silencing of ATP7A in Anx A4-overexpressing HEC1-A63 and HEC1-A77 cells resulted in greater intracellular platinum accumulation than HEC1-A63 and HEC1-A77 cells transfected with a control siRNA. On the other hand, the analysis of IC_{50} values for 5-FU showed no relationship between overexpression of Anx A4 and resistance to 5-FU. In addition, no improvement in sensitivity to 5-FU was observed as a result of ATP7A silencing. These results suggested a specific relationship of Anx A4 with ATP7A and resistance to platinum drugs but with to nonplatinum drugs such as 5-FU. Differences in efficacy and improvement in drug sensitivity of ATP7A silencing were observed between cell lines (HEC1, HEC1-CV, HEC1-A63 and HEC1-A77 cells). These variations may be related to the colocalization of Anx A4 and ATP7A in the cellular membrane after cisplatin or carboplatin exposure. Colocalization of Anx A4 and ATP7A after exposure to platinum drugs was specific to changes in Anx A4-overexpressing cells, which are probably related to drug efflux. These results suggest that in conjunction with higher Anx A4 expression levels, ATP7A had a positive effect on efflux of platinum drugs, resulting in significantly increased platinum resistance. Because overexpression of Anx A4 had no effect on ATP7A expression and because no direct interaction between ATP7A and Anx A4 was detected in the coimmunoprecipitation analysis, Anx A4 seems to promote ATP7A activity in a manner which is currently unexplained.

In addition to the effects of Anx A4 on drug resistance in ovarian cancer, similar findings have been reported for other overexpressed members of the Annexin family such as Annexin A3 (Anx A3).[46,47] Intracellular platinum concentrations of cisplatin and levels of platinum DNA binding in that study were significantly lower in Anx A3-overexpressing cells than in control cells, suggesting a more general involvement of the Annexin family in platinum resistance.[46] From the results of these related reports and those of our study, we conclude that the Annexin family may potentially enhance the activity of numerous drug transporters. Identifying these enhancement mechanisms may be extremely useful for developing additional therapeutic targets for drug-resistant tumors.

In summary, our study demonstrated that enhanced expression of Anx A4 induces chemoresistance by promoting platinum drug efflux *via* ATP7A. These findings suggested that Anx A4 is a potential therapeutic target for chemosensitization, particularly in tumors with higher expression of both Anx A4 and ATP7A. Thus, our study provides a clear example of applied genotoxicology. However, platinum resistance induced by overexpression of Anx A4 may occur as a

result of multiple processes, including regulation of apoptosis and efflux of platinum drugs. Thus, other unknown chemoresistant mechanisms may be induced by overexpression of Anx A4. Because overexpression of Anx A4 has been reported in several other types of clinically important cancers, such as rectal, renal, lung and pancreatic cancer,[19–23] targeting Anx A4 may lead to the development of an effective therapy for overcoming chemoresistance in more types of cancer.

Acknowledgements

The authors thank Y. Kanazawa and S. Sugiyama for their secretarial assistance, M. Urase for technical assistance and Dr. G.S. Buzard for helpful editing.

References

1. Omura G, Blessing JA, Ehrlich CE, et al. A randomized trial of cyclophosphamide and doxorubicin with or without cisplatin in advanced ovarian carcinoma. *A Gynecologic Oncology Group Study. Cancer* 1986;57:1725–30.
2. Thigpen T, Vance R, Puneky L, et al. Chemotherapy in advanced ovarian carcinoma: current standards of care based on randomized trials. *Gynecol Oncol* 1994;55:S97–S107.
3. Vaughan S, Coward JI, Bast RC, Jr, et al. Rethinking ovarian cancer: recommendations for improving outcomes. *Nat Rev Cancer* 2011;11: 719–25.
4. Fleming GF, Brunetto VL, Cella D, et al. Phase III trial of doxorubicin plus cisplatin with or without paclitaxel plus filgrastim in advanced endometrial carcinoma: a Gynecologic Oncology Group Study. *J Clin Oncol* 2004;22:2159–66.
5. Hoskins PJ, Swenerton KD, Pike JA, et al. Paclitaxel and carboplatin, alone or with irradiation, in advanced or recurrent endometrial cancer: a phase II study. *J Clin Oncol* 2001;19:4048–53.
6. Obel JC, Friberg G, Fleming GF. Chemotherapy in endometrial cancer. *Clin Adv Hematol Oncol* 2006;4:459–68.
7. Enomoto T, Kuragaki C, Yamasaki M, et al. Is clear cell carcinoma and mucinous carcinoma of the ovary sensitive to combination chemotherapy with paclitaxel and carboplatin? *Proc Am Soc Clin Oncol* 2003;22:(abstr 1797).
8. Nakayama K, Kanzaki A, Terada K, et al. Prognostic value of the Cu-transporting ATPase in ovarian carcinoma patients receiving cisplatin-based chemotherapy. *Clin Cancer Res* 2004;10: 2804–11.
9. Pectasides D, Fountzilas G, Aravantinos G, et al. Advanced stage clear-cell epithelial ovarian cancer: the Hellenic Cooperative Oncology Group experience. *Gynecol Oncol* 2006;102: 285–91.
10. Goff BA, Sainz de la Cuesta R, Muntz HG, et al. Clear cell carcinoma of the ovary: a distinct histologic type with poor prognosis and resistance to platinum-based chemotherapy in stage III disease. *Gynecol Oncol* 1996;60:412–17.
11. Sugiyama T, Kamura T, Kigawa J, et al. Clinical characteristics of clear cell carcinoma of the ovary: a distinct histologic type with poor prognosis and resistance to platinum-based chemotherapy. *Cancer* 2000;88:2584–9.
12. Kim A, Enomoto T, Serada S, et al. Enhanced expression of Annexin A4 in clear cell carcinoma of the ovary and its association with chemoresistance to carboplatin. *Int J Cancer* 2009;125: 2316–22.
13. Miao Y, Cai B, Liu L, et al. Annexin IV is differentially expressed in clear cell carcinoma of the ovary. *Int J Gynecol Cancer* 2009;19:1545–9.
14. Gerke V, Moss SE. Annexins: from structure to function. *Physiol Rev* 2002;82:331–71.
15. Kaetzel MA, Hazarika P, Dedman JR. Differential tissue expression of three 35-kDa annexin calcium-dependent phospholipid-binding proteins. *J Biol Chem* 1989;264:14463–70.
16. Kaetzel MA, Mo YD, Mealy TR, et al. Phosphorylation mutants elucidate the mechanism of annexin IV-mediated membrane aggregation. *Biochemistry* 2001;40:4192–9.
17. Kim A, Serada S, Enomoto T, et al. Targeting annexin A4 to counteract chemoresistance in clear cell carcinoma of the ovary. *Expert Opin Ther Targets* 2010;14:963–71.
18. Jeon YJ, Kim DH, Jung H, et al. Annexin A4 interacts with the NF-kappaB p50 subunit and modulates NF-kappaB transcriptional activity in a Ca2+-dependent manner. *Cell Mol Life Sci* 2010; 67:2271–81.
19. Alfonso P, Canamero M, Fernandez-Carbonie F, et al. Proteome analysis of membrane fractions in colorectal carcinomas by using 2D-DIGE saturation labeling. *J Proteome Res* 2008;7:4247–55.
20. Duncan R, Carpenter B, Main LC, et al. Characterisation and protein expression profiling of annexins in colorectal cancer. *Br J Cancer* 2008; 98:426–33.
21. Sitek B, Luttges J, Marcus K, et al. Application of fluorescence difference gel electrophoresis saturation labelling for the analysis of microdissected precursor lesions of pancreatic ductal adenocarcinoma. *Proteomics* 2005;5:2665–79.
22. Zimmermann U, Balabanov S, Giebel J, et al. Increased expression and altered location of annexin IV in renal clear cell carcinoma: a possible role in tumour dissemination. *Cancer Lett* 2004;209:111–18.
23. Wei R, Zhang Y, Shen L, et al. Comparative proteomic and radiobiological analyses in human lung adenocarcinoma cells. *Mol Cell Biochem* 2012;359:151–9.
24. Furukawa T, Komatsu M, Ikeda R, et al. Copper transport systems are involved in multidrug resistance and drug transport. *Curr Med Chem* 2008;15:3268–78.
25. Gourdon P, Liu XY, Skjorringe T, et al. Crystal structure of a copper-transporting PIB-type ATPase. *Nature* 2011;475:59–64.
26. Owatari S, Akune S, Komatsu M, et al. Copper-transporting P-type ATPase, ATP7A, confers multidrug resistance and its expression is related to resistance to SN-38 in clinical colon cancer. *Cancer Res* 2007;67:4860–8.
27. Samimi G, Varki NM, Wilczynski S, et al. Increase in expression of the copper transporter ATP7A during platinum drug-based treatment is associated with poor survival in ovarian cancer patients. *Clin Cancer Res* 2003;9:5853–9.
28. Safaei R, Holzer AK, Katano K, et al. The role of copper transporters in the development of resistance to Pt drugs. *J Inorg Biochem* 2004;98: 1607–13.
29. Iwahori K, Serada S, Fujimoto M, et al. SOCS-1 gene delivery cooperates with cisplatin plus pemetrexed to exhibit preclinical antitumor activity against malignant pleural mesothelioma. *Int J Cancer* 2013;132:459–71.
30. Khunweeraphong N, Nagamori S, Wiriyasermkul P, et al. Establishment of stable cell lines with high expression of heterodimers of human 4F2hc and human amino acid transporter LAT1 or LAT2 and delineation of their differential interaction with (alpha)-alkyl moieties. *J Pharmacol Sci* 2012;119:368–80.
31. Rabik CA, Maryon EB, Kasza K, et al. Role of copper transporters in resistance to platinating agents. *Cancer Chemother Pharmacol* 2009;64: 133–42.
32. Galluzzi L, Senovilla L, Vitale I, et al. Molecular mechanisms of cisplatin resistance. *Oncogene* 2012;31:1869–83.
33. Kelland L. The resurgence of platinum-based cancer chemotherapy. *Nat Rev Cancer* 2007;7:573–84.
34. Arts HJ, Katsaros D, de Vries EG, et al. Drug resistance-associated markers P-glycoprotein, multidrug resistance-associated protein 1, multidrug resistance-associated protein 2, and lung resistance protein as prognostic factors in ovarian carcinoma. *Clin Cancer Res* 1999;5:2798–805.
35. Guminski AD, Balleine RL, Chiew YE, et al. MRP2 (ABCC2) and cisplatin sensitivity in hepatocytes and human ovarian carcinoma. *Gynecol Oncol* 2006;100:239–46.
36. Materna V, Pleger J, Hoffmann U, et al. RNA expression of MDR1/P-glycoprotein, DNA-topoisomerase I, and MRP2 in ovarian carcinoma patients: correlation with chemotherapeutic response. *Gynecol Oncol* 2004;94:152–60.
37. Aida T, Takebayashi Y, Shimizu T, et al. Expression of copper-transporting P-type adenosine triphosphatase (ATP7B) as a prognostic factor in human endometrial carcinoma. *Gynecol Oncol* 2005;97:41–5.
38. Katano K, Kondo A, Safaei R, et al. Acquisition of resistance to cisplatin is accompanied by changes in the cellular pharmacology of copper. *Cancer Res* 2002;62:6559–65.
39. Kuo MT, Chen HH, Song IS, et al. The roles of copper transporters in cisplatin resistance. *Cancer Metastasis Rev* 2007;26:71–83.
40. Samimi G, Safaei R, Katano K, et al. Increased expression of the copper efflux transporter ATP7A mediates resistance to cisplatin, carboplatin, and oxaliplatin in ovarian cancer cells. *Clin Cancer Res* 2004;10:4661–9.
41. Mangala LS, Zuzel V, Schmandt R, et al. Therapeutic targeting of ATP7B in ovarian carcinoma. *Clin Cancer Res* 2009;15:3770–80.
42. Kalayda GV, Wagner CH, Buss I, et al. Altered localisation of the copper efflux transporters ATP7A and ATP7B associated with cisplatin

resistance in human ovarian carcinoma cells. *BMC Cancer* 2008;8:175.
43. Al-Bahlani S, Fraser M, Wong AY, et al. P73 regulates cisplatin-induced apoptosis in ovarian cancer cells via a calcium/calpain-dependent mechanism. *Oncogene* 2011;30:4219–30.
44. Splettstoesser F, Florea AM, Busselberg D. IP(3) receptor antagonist, 2-APB, attenuates cisplatin induced Ca2+-influx in HeLa-S3 cells and prevents activation of calpain and induction of apoptosis. *Br J Pharmacol* 2007;151: 1176–86.
45. Choi CH, Sung CO, Kim HJ, et al. Overexpression of annexin A4 is associated with chemoresistance in papillary serous adenocarcinoma of the ovary. *Hum Pathol* 2013;44:1017–23.
46. Yan X, Yin J, Yao H, et al. Increased expression of annexin A3 is a mechanism of platinum resistance in ovarian cancer. *Cancer Res* 2010;70:1616–24.
47. Yin J, Yan X, Yao X, et al. Secretion of annexin A3 from ovarian cancer cells and its association with platinum resistance in ovarian cancer patients. *J Cell Mol Med* 2012;16:337–48.

Journal of Virology

Varicella-Zoster Virus ORF49 Functions in the Efficient Production of Progeny Virus through Its Interaction with Essential Tegument Protein ORF44

Tomohiko Sadaoka, Satoshi Serada, Junko Kato, Mayuko Hayashi, Yasuyuki Gomi, Tetsuji Naka, Koichi Yamanishi and Yasuko Mori

J. Virol. **2014, 88(1):188. DOI: 10.1128/JVI.02245-13.**
Published Ahead of Print 23 October 2013.

JVI
Journals.ASM.org

Varicella-Zoster Virus ORF49 Functions in the Efficient Production of Progeny Virus through Its Interaction with Essential Tegument Protein ORF44

Tomohiko Sadaoka,[a,b] Satoshi Serada,[c] Junko Kato,[a] Mayuko Hayashi,[a,b] Yasuyuki Gomi,[d] Tetsuji Naka,[c] Koichi Yamanishi,[e] Yasuko Mori[a,b]

Division of Clinical Virology, Center for Infectious Diseases, Kobe University Graduate School of Medicine, Kusunoki-cho, Chuo-ku, Kobe, Japan[a]; Laboratory of Virology and Vaccinology, Division of Biomedical Research, National Institute of Biomedical Innovation, Saito-Asagi, Ibaraki, Osaka, Japan[b]; Laboratory of Immune Signal, Division of Biomedical Research, National Institute of Biomedical Innovation, Saito-Asagi, Ibaraki, Osaka, Japan[c]; Kanonji Institute, The Research Foundation for Microbial Diseases of Osaka University, Kanonji, Kagawa, Japan[d]; National Institute of Biomedical Innovation, Saito-Asagi, Ibaraki, Osaka, Japan[e]

The ORF49 tegument protein of varicella-zoster virus (VZV) is one of the core gene products that is conserved among herpesvirus family members. Although ORF49 is known to be a cell-tropic factor, its detailed functions remain elusive. ORF44 is another core gene product reported to be essential, although its characterization and detailed functional analysis have not been reported. These two core gene products form a complex in other herpesviruses beyond the host species and herpesvirus subfamilies. Here, we show that complex formation between ORF44 and ORF49 is conserved in VZV. We serendipitously found that binding is eliminated by an amino acid substitution at position 129 (phenylalanine 129), and four amino acids in the carboxyl-terminal half of the acidic cluster in ORF49 (i.e., aspartate-phenylalanine-aspartate-glutamate from positions 41 to 44 [41DFDE44]) were identified as its binding motif. Alanine substitutions in each domain rendered the ORF44F129A mutation lethal for VZV, similar to deletion of the entire ORF44. The phenotype of the ORF49-41AAAA44 mutation was comparable to that of the ORF49-defective virus, including small-plaque formation, impaired growth, and low infectious virus production. These results suggest that the interaction between ORF44 and ORF49 is essential for their role in VZV infection and that ORF49 is required for the efficient production of infectious progeny virus mediated by the conserved interaction between the two proteins.

Varicella-zoster virus (VZV) is a member of the human alphaherpesvirus subfamily and the etiologic agent of two diseases: varicella is the result of primary infection with VZV, and herpes zoster is caused by reactivation of the virus from the latent state (1). VZV shares many features, especially a tropism for epithelial and neural tissues, with other human alphaherpesvirus members, including herpes simplex viruses 1 and 2 (HSV-1 and -2, respectively), and with the nonhuman alphaherpesviruses. However, VZV spreads only via cell-to-cell infection in culture and is more akin to the betaherpesviruses (i.e., human herpesviruses 6 and 7) in its apparent T-cell-tropism (1).

The VZV genome is approximately 125 kb and contains at least 70 unique open reading frames (ORFs), and it is the smallest genome in terms of length and gene set among human herpesviruses (1–3). Of the 70 identified ORFs, 44 are core genes that are conserved among all human herpesvirus subfamilies (4). Recent genome-wide mutagenesis analysis showed that 34 ORFs among the core genes are essential for virus reconstitution in cell culture, whereas deletion of seven ORFs results in viral growth defects, and three ORFs are dispensable in cell culture or skin organ culture (5). Eight core genes encode tegument proteins, which are the structural components of the virion and are located between the nucleocapsid and the envelope.

VZV ORF49 encodes a nonessential tegument protein that functions as a cell-tropic factor in cell culture via an unknown mechanism (6). VZV ORF49 is the homolog of HSV-1 UL11 and human cytomegalovirus (HCMV) UL99, which are among the most extensively studied tegument protein-encoding genes. The UL11 and UL99 gene products, pUL11 and pp28, function in secondary envelopment (7–9), but they have different roles in the viral life cycle. HSV-1 UL11 is not essential for the viral life cycle; however, the UL11 deletion mutant forms small plaques, and the final titers are reduced to 80 to 95% of wild-type levels (10). In contrast, HCMV UL99 is an essential gene, and pp28-deficient mutants show extremely impaired growth in normal fibroblasts and produce no detectable infectious progeny (9). However, this mutant spreads from cell to cell via an unknown mechanism (11).

Several recent reports, beginning with one on HSV-1 UL16, which is a core gene within the intron of a conserved herpesvirus spliced gene, (12), showed that interactions between pUL11 and pUL16 homologs were conserved beyond the host species and herpesvirus subfamilies (13–15). HSV pUL16 localizes to the nucleus and the cytoplasm of infected cells and functions in virus entry and in nuclear and cytoplasmic egress (16–19); pUL16 homologs may function in secondary envelopment, as reviewed in reference 20. As described for UL11 homologs, whether UL16 homologs are required for the viral life cycle differs among viruses (13, 15, 21–25). In a genome-wide mutagenesis analysis, deletion of the entire gene region from the viral genome of VZV ORF44, the UL16 homolog, showed that it is an essential gene by loss-of-function analysis in the MeWo cell line (5), although this was not

Received 11 August 2013 Accepted 10 October 2013
Published ahead of print 23 October 2013
Address correspondence to Yasuko Mori, ymori@med.kobe-u.ac.jp.

doi:10.1128/JVI.02245-13

confirmed by a revertant virus generated for gain-of-function analysis.

The LI motif and the conserved acidic cluster of pUL11 are essential for its interaction with pUL16 of HSV-1, whereas the critical sequences in pUL16 have not been determined because it is highly sensitive to deletions. Its short N-terminal 75-amino-acid (aa) fragment was recently shown to include the pUL11 binding site, and its C-terminal region functions as the binding regulatory domain (26), although this has not been confirmed in the context of HSV-1-infection. HCMV pUL94 directs pp28 to the assembly compartment, where it plays a role in secondary envelopment. Amino acids 37 to 39, near the acidic cluster of pp28, and one of the conserved cysteine residues of pUL94 are involved in binding in the context of infection (24, 27). In VZV, potential ORF49 protein (ORF49p)-binding proteins, including the pUL16 homolog ORF44 protein (ORF44p), were identified by global screening using the yeast two-hybrid system (28, 29), although these interactions have not been confirmed, even by coexpression experiments in mammalian cells.

In our previous study on VZV ORF49 (6), ORF49p was identified as one of the cell-tropic factors for VZV lytic infection in cell culture. However, the precise function of ORF49 in cells in which the ORF49-defective virus showed impaired growth was not elucidated. To address this issue, we established a complete *trans*-complementation system for ORF49 and identified ORF44p as its binding partner in the context of infection. In the present study, we aimed to reveal the precise role of ORF49p by using this system and by analyzing the conserved mechanism of interaction between these proteins and its role in VZV infection.

MATERIALS AND METHODS

Cells and viruses. The melanoma cell line MeWo was propagated in Dulbecco's modified Eagle's medium (DMEM) (Nissui Pharmaceutical, Ueno, Tokyo) supplemented with 8% fetal bovine serum (FBS) (Sigma-Aldrich, St. Louis, MO), 0.6 mg/ml L-sodium glutamate, and 0.02 mg/ml gentamicin sulfate (Nacalai Tesque, Kyoto, Japan) (DMEM complete). MeWo cells stably expressing Cre recombinase, designated MeWo-Cre cells, were maintained in DMEM complete supplemented with 500 μg/ml G418 (Nacalai Tesque) (30). MeWoORF49 cells stably expressing ORF49 were generated as follows: MeWo cells were transfected with CAG/ORF49 (described below) using Lipofectamine 2000 (Invitrogen, Carlsbad, CA) according to the manufacturer's instructions, selected, and propagated in DMEM complete supplemented with 1.5 μg/ml puromycin (Invitrogen). Recombinant viruses derived from the parental VZV strain Oka (pOka), rpOka, rpOkaΔ44Rev, rpOkaORF44F129ARev, rpOkaORF44T128A, rpOkaORF44K130A, rpOkaORF49M1L, rpOkaORF49M1LRev, rpOka-ORF49-41AAAA44, and rpOkaORF49-41AAAA44Rev were maintained in DMEM complete supplemented with 3% FBS.

Cell-free virus was prepared as described previously with slight modifications (6). At 48 h postinfection (hpi) by cell-to-cell spread, cells were harvested with a cell scraper (Iwaki, Tokyo, Japan), spun at 800 × *g* for 5 min at 4°C, and suspended in SGP buffer (phosphate-buffered saline [PBS] containing 0.1% L-sodium glutamate and 7% sucrose). The suspended cells were treated with an ultrasonic disruptor (UD-201; Tomy Seiko, Tokyo, Japan) at 1.5° for 30 s on ice and spun at 800 × *g* for 5 min at 4°C, and the supernatant was stored at −80°C until use. The purified viral particles were prepared as described in reference 6. Briefly, the cell-free virus solutions were subjected to Histodenz (Sigma-Aldrich) gradient purification (5 to 50% in PBS) by ultracentrifugation at 50,200 × *g* for 2 h at 4°C in a P40ST rotor (CP80WX; Hitachi Koki, Hitachinaka, Japan). Aliquots of the peak particle-containing fractions were subjected to ultracentrifugation at 52,600 × *g* for 2 h at 4°C in a P28S rotor (CP80WX; Hitachi Koki), and the pellets were stored at −80°C for further analyses.

Plasmids. The pGEX/ORF44, pGEX/ORF44A, and pGEX/ORF44P plasmids were generated to express the full length (corresponding to aa 2 to 363), anterior half (aa 2 to 200), and posterior half (aa 181 to 363) of the ORF44 protein in *Escherichia coli*. The primer pairs ORF44ecoF4 (5′-ACCGAATTCGAATTACAACGCATATTTCCG-3′) and ORF44salR (5′-ACCGTCGACCTAGGTGGTTGTAGG-3′) for ORF44, ORF44ecoF4 and ORF44salR600 (5′-ACCGTCGACTAAATTAGGTTCCATAGCC-3′) for ORF44A, and ORF44ecoF541 (5′-ACCGAATTCGGAGTGTGGTGGTCAGACG-3′) and ORF44salR for ORF44P were used to amplify each indicated region of the ORF44 gene from the rpOka cDNA. The PCR products were inserted in frame into the pGEX6P-1 bacterial expression vector (GE Healthcare Bio-Sciences, Piscataway, NJ) via the EcoRI and SalI sites (underlined). The same procedure was used to construct pGEX/ORF61. The DNA fragment (positions 406 to 744) of ORF61 was cloned into pGEX6P-1 via the BamHI and SalI sites (underlined). The primer pair was ORF61bamF406 (5′-ACCGGATCCGGGCCCCTTCAATCGTCGG-3′) and ORF61salR744stop (5′-ACCGTCGACCTAGAATCTCGCGTTTCCCTC-3′). The eukaryotic ORF44 expression plasmid CAG/ORF44 or CAG/FLAGORF44, which was N-terminally tagged with FLAG (DYKDDDDK), was generated as follows: the entire ORF44 gene was amplified by PCR with the primers ORF44-25kpnF (5′-ACCGGTACCAATCCGCTAGACTG-3′) or ORF44FLAGkpnF4 (5′-ACCGGTACCGCCACCATGgactacaaagacgatgacgacaagGAATTACAACGCATATTTCCG-3′) and ORF44salR, and the PCR fragment was cut by KpnI and SalI (underlined) and cloned into pCAGGS-MCS-neo via the KpnI and XhoI sites. The FLAG tag coding sequence within the primer for ORF44FLAGkpnF4 is shown in lowercase letters. The ORF49 expression plasmid CAG/ORF49 was generated as follows: the entire ORF49 gene was amplified by PCR with the primers ORF49-24ecoF (5′-ACCGAATTCTTACATCAGCATTGCG−3′) and ORF49bamR (5′-ACCGGATCCTTAACATTTTGCGCATTTGG-3′), and the PCR fragment was cut by EcoRI and BamHI (underlined) and cloned into pCAGGS-MCS-puro via the EcoRI and BglII sites. The pCAGGS plasmid was kindly provided by Jun-ichi Miyazaki (Osaka University, Japan) (31). A Cre recombinase-expressing plasmid, pCX-Cre-neo, was previously generated (30) from pCX-Cre, which was a generous gift from Masaru Okabe (Osaka University, Japan).

Construction of mutant ORF44 and ORF49 expression plasmids. The ORF44 mutant plasmids pGEX/ORF44F129A, CAG/ORF44T128A, CAG/ORF44F129A, CAG/ORF44K130A, CAG/FLAGORF44I121stop, CAG/FLAGORF44P136stop, and CAG/FLAGORF44F129AP136stop and the ORF49 mutant plasmid CAG/ORF49-41AAAA44 were generated with a QuikChange Lightning multisite-directed mutagenesis kit (Agilent Technologies, La Jolla, CA) according to the manufacturer's recommendations, using the primers listed in Table 1 based on pGEX/ORF44, CAG/ORF44, CAG/FLAGORF44, and CAG/ORF49, respectively. The ORF49 C-terminal deletion mutant plasmids CAG/ORF49N40, CAG/ORF49N44, and CAG/ORF49N48 were generated using the following primer pairs: ORF49-24ecoF (5′-ACCGAATTCTTACATCAGCATTGCG-3′) as the forward primer for all the deletion mutants and ORF49mycxhoR120 (5′-ACCCTCGAGcagatcctcttctgagatgagtttttgttcAAAGTCTTCAAAGAACTCTG-3′), ORF49mycxhoR132 (5′-ACCCTCGAGcagatcctcttctgagatgagtttttgttcCTCATCAAAGTCAAAGTCTT-3′), or ORF49mycxhoR144 (5′-ACCCTCGAGcagatcctcttctgagatgag tttttgttcCTCTGTTACATTCTCATCAAAGTC-3′) as the reverse primer for CAG/ORF49N40, CAG/ORF49N44, or CAG/ORF49N48. All of the reverse primers contained a c-myc tag, indicated by lowercase letters, and the PCR products were cloned into pCAGGS-MCS-puro via the EcoRI and XhoI sites (underlined).

Antibodies. To produce a mouse monoclonal antibody (MAb) against ORF44, a glutathione *S*-transferase (GST)-ORF44A recombinant protein was expressed in *E. coli* BL21 transformed with pGEX/ORF44A, purified, and used to immunize mice; hybridoma clones producing the anti-ORF44 MAb were established as described previously (32). To produce polyclonal anti-ORF61 Abs, a GST-ORF61 fusion protein was purified from *E. coli* BL21 transformed with pGEX-ORF61 and used to immunize a rabbit

TABLE 1 Primers used for ORF44 or ORF49 mutations

Primer	Sequence[a]	Amino acid substitution(s)
ORF44 361at-ta	5′-TAT CCG GTT GAA AAC TAA GAC CAT GTT TTT GGA-3′	Ile 121 to stop (TAA)
ORF44 382a-g	5′-CAT GTT TTT GGA GCA GCG TTT AAG AAC CC-3′	Thr 128 to Ala
ORF44 385tt-gc	5′-TT TTT GGA GCA ACG GCT AAG AAC CCG ATC G-3′	Phe 129 to Ala
ORF44 388aa-gc	5′-TTT GGA GCA ACG TTT GCG AAC CCG ATC GCG-3′	Lys 130 to Ala
ORF44 406ccc-taa	5′-AAC CCG ATC GCG TAC TAA CTT CCA ACA TCT ATT-3′	Pro 136 to stop (TAA)
ORF49 M1L	5′-ATT GCG GTC ATT GCG TTG GGA CAA TCT TCA-3′	Met 1 to Leu
ORF49 41AAAA44	5′-TTT GAA GAC TTT GCC GCT GCT GCG AAT GTA ACA GAG-3′	Asp-Phe-Asp-Glu (41–44) to Ala-Ala-Ala-Ala

[a] Nucleotides that differ from those of the wild type are underlined.

(Sigma Genosys, Hokkaido, Japan). The anti-ORF61 Ab was purified with GST-conjugated normal human serum (NHS)-activated Sepharose and GST-ORF61-conjugated NHS-activated Sepharose. Rabbit polyclonal anti-ORF49 and anti-gB-C Abs were described previously (6). The mouse anti-glycoprotein E (anti-gE) (clone 9) Ab was described in reference 33. Mouse anti-glycoprotein H (gH) (VgIII-3) was obtained as described previously (33). Sheep anti-*trans*-Golgi network (anti-TGN46) Ab (AHP500G; AbD Serotec, Oxford, United Kingdom), anti-α-tubulin Ab (B-5-1-2; Sigma-Aldrich), and goat anti-GST Ab (GE Healthcare Bio-Sciences) were commercially available. Alexa Fluor 488-labeled donkey anti-mouse immunoglobulin G (IgG), Alexa Fluor 594-labeled donkey anti-rabbit IgG, and Alexa Fluor 647-labeled donkey anti-sheep IgG (Invitrogen) were used as secondary Abs, and Hoechst 33342 (Sigma-Aldrich) was used for nuclear staining in confocal microscopic analyses. ECL enhanced chemiluminescence anti-mouse or anti-rabbit IgG horseradish peroxidase-linked whole antibodies from donkey (GE Healthcare Bio-Sciences) were used as secondary Abs in immunoblotting.

Mutagenesis of viral genomes in *E. coli*. The mutant bacterial artificial chromosomes (BACs) pOka-BACORF49M1L, containing a methionine-to-leucine substitution at residue Met-1, and pOka-BACORF49-41AAAA44, containing a tetra-alanine substitution at residues 41-Asp-Phe-Asp-Glu-44, were generated by *recA*-mediated allelic replacement in pOka-BAC-harboring DH10B transformed with pST76A-SR/pOkaORF49M1L and pST76A-SR/pOkaORF49-41AAAA44, respectively, which were derived from pST76A-SR/pOkaORF50 (including nucleotide positions 84361 to 89970 of pOka) (30), using the primers listed in Table 1 and a QuikChange Lightning multisite-directed mutagenesis kit. The revertant BACs pOka-BACORF49M1LRev and pOkaBACORF49-41AAAA44Rev were generated by recA-mediated allelic replacement using pST76A-SRORF50 transformed into DH10B cells harboring pOka-BACORF49M1L and pOka-BACORF49-41AAAA44, respectively.

To generate pOka-BACΔ44, in which the nucleotides (nt) 1 to 800 of the ORF44 gene were replaced with an FRT (*flp* recombinase recognition target) sequence, a linear fragment was amplified by PCR using the primer pair ORF44FRTfKMF0 (5′-TTAAACCCACAAGTACC CGGGCGGCAATCCGCTAGACTGTTTTTCTGCTCGAAGTTCCTA TTCTCTAGAAAGTATAGGAACTTCAGCAAGCGAACCGGAAT TGC-3′) and ORF44FRTrKMR800 (5′-TCCCGCTGACCGGCCTTT CTCCACATACACGGAGCCCAACACACACAACCGAAGTTCCTAT ACTTTCTAGAGAATAGGAACTTCCTTTTTCAATTCAGAAGA ACTC-3′) (FRT is underlined) using pCR2.1-TOPO as the template (Invitrogen). The amplified fragment was then transformed into DH10B harboring pOka-BAC (34) with pGETrec (a kind gift from Panayiotis A. Ioannou, The Murdoch Institute for Research into Birth Defects, Royal Children's Hospital, Melbourne, Australia) (35); *recE/T* recombination for pOka-BACΔ44KMr and excision of the kanamycin resistance gene from pOka-BACΔ44KMr by the *flp*/FRT system using pCP20 (a kind gift from Wilfried Wackernagel, Universität Oldenburg, Germany) (36), resulting in pOka-BACΔ44, were carried out as described previously (6).

To construct pOka-BACΔ44Rev, the revertant BAC genome against pOka-BACΔ44, *recA*-mediated mutagenesis was performed as described previously (30), using the shuttle plasmid pST76A-SR/pOkaORF44. For pST76A-SR/pOkaORF44, a 3.2-kbp fragment of viral DNA corresponding to nt 79230 to 82453 of pOka was amplified from the pOka-BAC genome using the primer pair ORF43F1201 (5′-ACCGCTGCGTGTATA AATGCCCGGGTTGAC-3′) and ORF42/45F (5′-ACCATGTCATTGAT AATGTTTGG-3′), cloned into pCR2.1-TOPO, sequenced, cut with EcoRI, blunted, and cloned into the plasmid pST76A-SR (kindly provided by Ulrich H. Koszinowski, Max von Pettenkofer Institut, Ludwig-Maximilians-Universität München, Munich, Germany) (37), which was cut with KpnI and blunted.

The shuttle plasmids for the ORF44 point mutant BACs, pST76A-SRORF44T128A (with an alanine substitution for threonine at residue Thr-128), pST76A-SR/pOkaORF44F129A (with an alanine substitution for phenylalanine at residue Phe-129), and pST76A-SR/pOkaORF44K130A (with an alanine substitution for lysine at residue Lys-130), were generated from pST76A-SR/pOkaORF44 with a QuikChange Lightning multisite-directed mutagenesis kit using the primers listed in Table 1. Each mutated shuttle plasmid was transformed into DH10B harboring pOka-BACΔ44KMr, and *recA*-mediated allelic replacement was performed as described elsewhere (30) to generate pOka-BACORF44T128A, pOka-BACORF44F129A, and pOka-BACORF44K130A. The revertant BAC for the ORF44F129A mutant BAC, pOka-BACORF44F129ARev, was generated by *recA*-mediated allelic replacement using pST76A-SRORF44 transformed into pOka-BACORF44F129A-harboring DH10B.

All of the purified BACs were digested with BamHI or EcoRI to ensure that the expected DNA fragments were present, and the whole region for allelic replacement was sequenced to ensure that unexpected deletions or substitutions were not present.

Reconstitution of recombinant viruses and excision of the BAC cassette. MeWo cells or MeWoORF49 cells for rpOkaORF49M1L and rpOkaORF49-41AAAA44 seeded in one well of a 12-well plate were transfected with 3 μg of BAC DNA using Lipofectamine 2000 or X-treamGene HP (Roche Applied Science, Basel, Switzerland). After typical cytopathic effects (CPE) were seen in cells expressing green fluorescent protein (GFP), cell-free virus was prepared as described above and used to infect MeWo-Cre cells or pCX-Cre-neo-transfected MeWoORF49 cells for rpOkaORF49M1L and rpOkaORF49-41AAAA44 to excise the BAC cassette.

Immunoblotting, immunoprecipitation, and immunofluorescence. Immunoblotting, immunoprecipitation, and immunofluorescence were performed as described previously (30, 32) with slight modifications. The proteins in immunoblots were visualized by Chemi-Lumi One Super (Nacalai Tesque) in combination with LAS4000mini (GE Healthcare Bio-Sciences). Radioimmunoprecipitation assay (RIPA) lysis buffer (0.01 M Tris-HCl [pH 7.4], 0.15 M NaCl, 1% sodium deoxycholate, 1% Nonidet P-40, 0.1% SDS, 1 mM EDTA) supplemented with protease inhibitor cocktail (Sigma-Aldrich) was used for cell lysis, and the supernatants obtained by ultracentrifugation at 216,900 × *g* for 1 h at 4°C in a P50A3 rotor (CP80WX; Hitachi Koki) and precleared with protein G Sepharose 4 Fast Flow (GE Healthcare Bio-Sciences) were used for immunoblotting and immunoprecipitation. Immunofluorescence images were captured and analyzed by an FV1000D confocal microscope (Olympus, Tokyo, Japan).